STATE OF ALASKA

DEPARTMENT OF NATURAL RESOURCES

DIVISION OF GEOLOGICAL AND GEOPHYSICAL SURVEYS

Bill Sheffield — *Governor*

Esther Wunnicke — *Commissioner*

Ross G. Schaff — *State Geologist*

March 1983

The author is solely responsible for its content and will appreciate candid comments on the accuracy of the data as well as suggestions to improve the report.

Alaska Report of Investigations 83-2

PETROLOGY, GEOCHEMISTRY, AND ISOTOPE GEOCHRONOLOGY OF THE GILMORE DOME AND PEDRO DOME PLUTONS, FAIRBANKS MINING DISTRICT, ALASKA

By
J.D. Blum

STATE OF ALASKA
Department of Natural Resources
DIVISION OF GEOLOGICAL & GEOPHYSICAL SURVEY

According to Alaska Statute 41, the Alaska Division of Geological and Geophysical Surveys is charged with conducting 'geological and geophysical surveys to determine the potential of Alaska lands for production of metals, minerals, fuels, and geothermal resources; the locations and supplies of ground waters and construction materials; the potential geologic hazards to buildings, roads, bridges, and other installations and structures; and shall conduct other surveys and investigations as will advance knowledge of the geology of Alaska.'

In addition, the Division shall collect, evaluate, and publish data on the underground, surface, and coastal waters of the state. It shall also file data from well-drilling logs.

DGGS performs numerous functions, all under the direction of the State Geologist---resource investigations (including mineral, petroleum, geothermal, and water), geologic-hazard and geochemical investigations, and information services.

Administrative functions are performed under the direction of the State Geologist, who maintains his office in Anchorage. (3001 Porcupine Dr., 99501, ph 274-9681).

This report is for sale by DGGS for $2. It may be inspected at any of the four DGGS information offices: Alaska National Bank of the North Bldg., Geist Rd. and University Ave., Fairbanks; 3601 C St. (10th Floor), Anchorage; 230 So. Franklin St. (4th Floor), Juneau; and the State Office Bldg., Ketchikan. Mail orders should be addressed to DGGS, P.O. Box 80007, College, AK 99708.

FOREWORD

At the request of the Fairbanks North Star Borough, a study of the Livengood and Fairbanks mineral districts was undertaken by the University of Alaska and the Alaska Division of Geological and Geophysical Surveys (DGGS). The research team included both university staff and graduate students and DGGS personnel. Efforts were focused on the Fairbanks mining district during the first year of the program. This report discusses the petrology, geochemistry, and isotope geochronology of intrusive rocks in the Fairbanks mining district.

DGGS is pleased to have supported this study and to release the results as part of the Report of Investigations series.

R.G. Schaff
State Geologist

CONTENTS

Page

FIGURES

TABLES

PETROLOGY, GEOCHEMISTRY, AND ISOTOPE GEOCHRONOLOGY OF THE GILMORE DOME AND PEDRO DOME PLUTONS, FAIRBANKS MINING DISTRICT, ALASKA

By
J. D. Blum

ABSTRACT

A study of the geochemical and petrologic characteristics of intrusive rocks in the Fairbanks mining district was undertaken as part of the geologic and mineral-resource investigations of the area. Intrusive rocks in the Fairbanks mining district occur mainly as northeast-trending bodies that range in composition from granodiorite to quartz monzonite. Analysis of modal point-count, major-oxide, and trace-element data indicates that the plutons represent a comagmatic fractionation suite. Comparison of aplite-dike compositions to the synthetic granite system yield depth-of-emplacement estimates of about 4 km. A rubidium-strontium isochron for the plutons yielded an age of 91.0 ± 0.7 m.y.; previously determined potassium-argon dates are 90.7 ± 5.1 m.y. and 93.0 ± 5.0 m.y. This indicates that the rocks have not undergone a thermal resetting of the potassium-argon age since the time of emplacement. The initial $^{87}Sr/^{86}Sr$ ratio is 0.71238, which rules out juvenile sources for the magma and suggests that the rocks are primarily derived from remelted Precambrian crustal rocks.

Petrologic constraints in this study imply that tungsten concentrations near the Gilmore Dome stock were remobilized from presently exposed schists by hydrothermal processes associated with the stock, or alternatively were derived by anatectic melting of tungsten-bearing high-grade metamorphic rocks much deeper than the present erosion level and reconcentrated during crystallization of the magma.

INTRODUCTION

Purpose and Scope

This report summarizes a comprehensive investigation of the geochemical and petrologic characteristics of intrusive rocks in the Fairbanks mining district of interior Alaska. An understanding of geochemical and petrographic characteristics, time and depth of emplacement, crystallization history, and origin of the magmas is essential to gain a thorough understanding of the geologic history of the district. Detailed field mapping, major- and minor-element geochemical analysis, radiogenic isotope studies, and petrographic studies were used to determine the characteristics of the intrusive rocks. Detailed geologic maps of the Fairbanks mining district (completed as part of the comprehensive study) include DGGS Open-file Reports 146 (Robinson, 1982), -154 (Metz, 1982), -155 (Bundtzen, 1982), and -170 (Forbes and Weber, 1982). Detailed mapping of the Gilmore Dome pluton is shown on AOF-146.

Geography

The study area is located in the Fairbanks mining district, 20 km northeast of Fairbanks, Alaska, in the Yukon-Tanana Upland (fig. 1). The

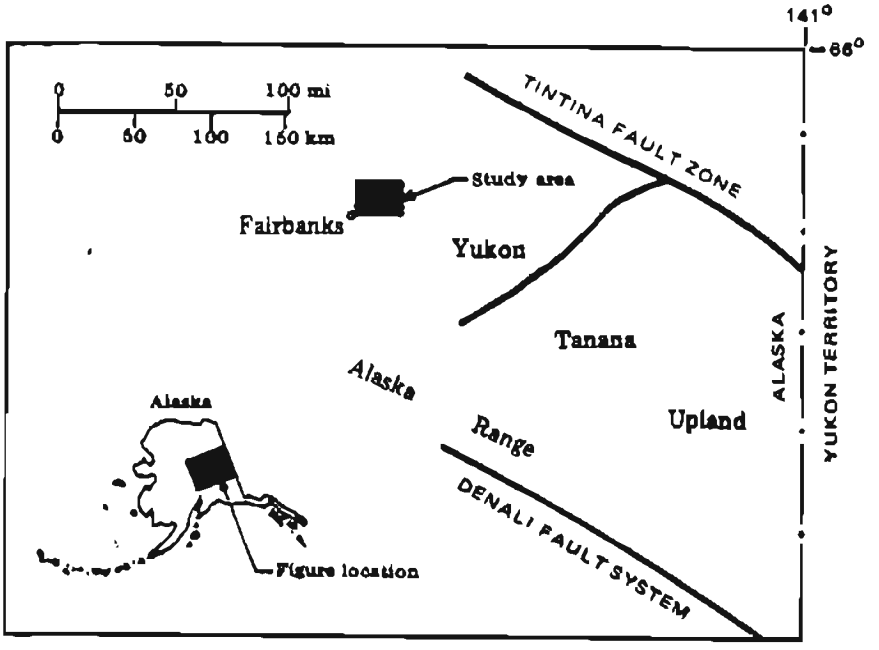

Figure 1. Location map of study area.

plutons crop out in an area of rolling hills that have a maximum relief of about 600 m and are covered with forest, brush, and tundra typical of subarctic regions. Outcrops are very rare, occur along ridges and in stream valleys, and are deeply weathered; they account for much less than 1 percent of the field area. The Pedro Dome area is readily accessible via the Steese and Elliot Highways and a network of unimproved roads leading to claims and prospects in the area. The Gilmore Dome area is accessible only from Gilmore Trail Road to the west and Gilmore Dome Road to the north.

Previous Investigations

Geologic studies of the Fairbanks mining district began in 1903 when a systematic geologic investigation of the Yukon-Tanana Upland was initiated by the U.S. Geological Survey under the direction of A.H. Brooks. Work under the direction of L.M. Prindle resulted in the first geologic description of the Fairbanks mining district (Prindle and others, 1913). From 1911 until 1931, J.B. Mertie, Jr., conducted a more extensive study of the geology of the Yukon-Tanana region and summarized the available geologic information (Mertie, 1937). Interest in tungsten and antimony during and after World War II prompted investigations of scheelite and stibnite deposits in the Pedro Dome and Gilmore Dome areas (Thorne and others, 1948; Byers, 1957). Several

detailed geologic investigations in the district were conducted by Forbes and Brown (1961) and Brown (1962) that centered on the Pedro Dome area. This work contributed much to the understanding of the outcrop pattern, structure, and petrology of the various rock units in the area. Forbes and others (1968) examined the gold gradients in relation to the intrusive bodies in the same area. Britton (1970) described the rocks of the Pedro Dome intrusive complex and illustrated the various igneous textures found in the Pedro Dome plutons. Britton's work is the only detailed petrologic study of intrusive rocks in the Fairbanks district to date. Forbes (1982) authored a comprehensive description of the geology and petrology of the Fairbanks mining district.

Regional Geology

The metamorphic rocks underlying the Fairbanks mining district have been assigned to the Yukon-Tanana metamorphic complex (Foster and others, 1973). The rocks are predominantly pelitic schists with lesser amounts of mafic and calc-silicate schists. The metamorphic mineral assemblages are low grade as defined by Winkler (1979). The parent rocks are sedimentary and volcanic rock types believed to be of late Proterozoic age (Wasserburg and others, 1963; Aleinikoff and others, 1981; Forbes, 1982).

The rocks are dominated by quartz-mica schists and micaceous quartzites, with subordinate felspathic schists, hornblende schists, calc-magnesian schists, and marbles. The metamorphic rocks are polydeformed and tectonized. Mesoscopic to megascopic, northwest-trending isoclinal-recumbent folds and mineral lineations define an early deformational event in the Yukon-Tanana Upland. Superimposed on these structures are large northeast-trending antiforms and synforms that record a refolding of earlier structures and define the most recent structural fabric in the region (Forbes, 1982). Granodiorite and quartz monzonite plutons intruded the metamorphic country rocks during the waning stages of the last major deformational period (Late Cretaceous time). The Gilmore Dome and Pedro Dome plutons have an elongate outcrop geometry that trends northeasterly and parallels the axial trace of the two dominant antiforms, suggesting structural control of magma emplacement.

Acknowledgments

I wish to thank P.A. Metz for suggesting this project and the Mineral Industry Research Laboratory (University of Alaska, Fairbanks) for providing logistical and laboratory support. M.H. Hall, J.D. Romick, W.I. Witte, and A.E. Blum aided me greatly through discussions of the research and assistance in sample collection. Thanks are also extended to D.B. Stone, D.B. Hawkins, and T.E. Smith for their critical reviews of the text. I am indebted to S.E. Swanson for his guidance through all phases of the research project, and for his support, constructive criticism, and review.

SAMPLE COLLECTION AND ANALYTICAL METHODS

Sampling Procedure

All intrusive rock samples are from generally fresh and unweathered rubble-crop that sparsely covers about half the field area. Most available

rock is displaced somewhat from its bedrock source and, for this reason, all sample locations and intrusive contacts are only approximate. The few outcrops that do exist are deeply weathered and were therefore inappropriate for chemical analysis. Sample locations were largely dictated by availability of rubble, but an attempt was made to maintain an approximate 1-km sample spacing. Sample locations are shown on figure 2 and listed by latitude and longitude in appendix A. Individual samples that weighed approximately 2 kg were collected, and samples that were too weathered to hold together during sawing were discarded. From each coherent sample, a rock slab for staining and a plug for a thin section were cut. The remaining rock from each sample was crushed, and a split (subsample) was pulverized. This split was used for trace-element and major-oxide analysis. Samples of coarse-grained rocks that weighed about 30 kg were collected and analyzed for rubidium and strontium isotopes. These were crushed and a split was pulverized.

Stained Slabs

Seventy-nine rock slabs cut from samples from the Gilmore-Pedro plutons were ground with No. 600 grit on a lab wheel, impregnated with molten Lakeside cement to fill cracks and pits, and repolished to remove excess cement. The rock slabs were then stained according to standard techniques described by Laniz and others (1964).

The slabs were point-counted under a microscope using an overlay grid of dots on clear acetate. Four hundred points per specimen were counted except for a few slabs whose surface areas limited the number of points counted to totals as low as 300. Because the best spacing for a given rock is equal to the size of the largest mineral grain in that rock (Van Der Plas and Tobi, 1965), a grid spacing of 8 mm was used for samples of porphyritic quartz monzonite, a grid spacing of 5 mm was used for samples of porphyritic granodiorite, and a grid spacing of 1 mm was used for samples of fine-grained granodiorite and aplitic rocks.

Van Der Plas and Tobi (1965) discuss the statistical reliability of point counting results and constructed a chart for determining the standard deviation of calculated modal percentages. The standard deviation is given within a 95-percent-confidence level for each combination of number of points counted and true content of a particular mineral. The relationship between standard deviation and true content of a mineral in percent-by-volume for a 400-point count is listed in appendix B. Standard deviation varies from 2 to 5 percent as the true content of a given mineral varies from 5 to 50 percent for 400 points. The content of potassium feldspar, plagioclase, quartz, and mafics was determined as percent by volume. The relative proportions of biotite, hornblende, pyroxene, chlorite, epidote, and sphene were later allocated from the percentage of total mafics by estimation from thin sections. Because primary white mica was indistinguishable from quartz on the slabs, its percentage was estimated in thin section and subtracted from that of quartz.

Before the point-count data could be used to discuss modal variations within and among the Gilmore-Pedro plutons, it was necessary to determine the magnitude of within-outcrop modal variation. Only modal variations between

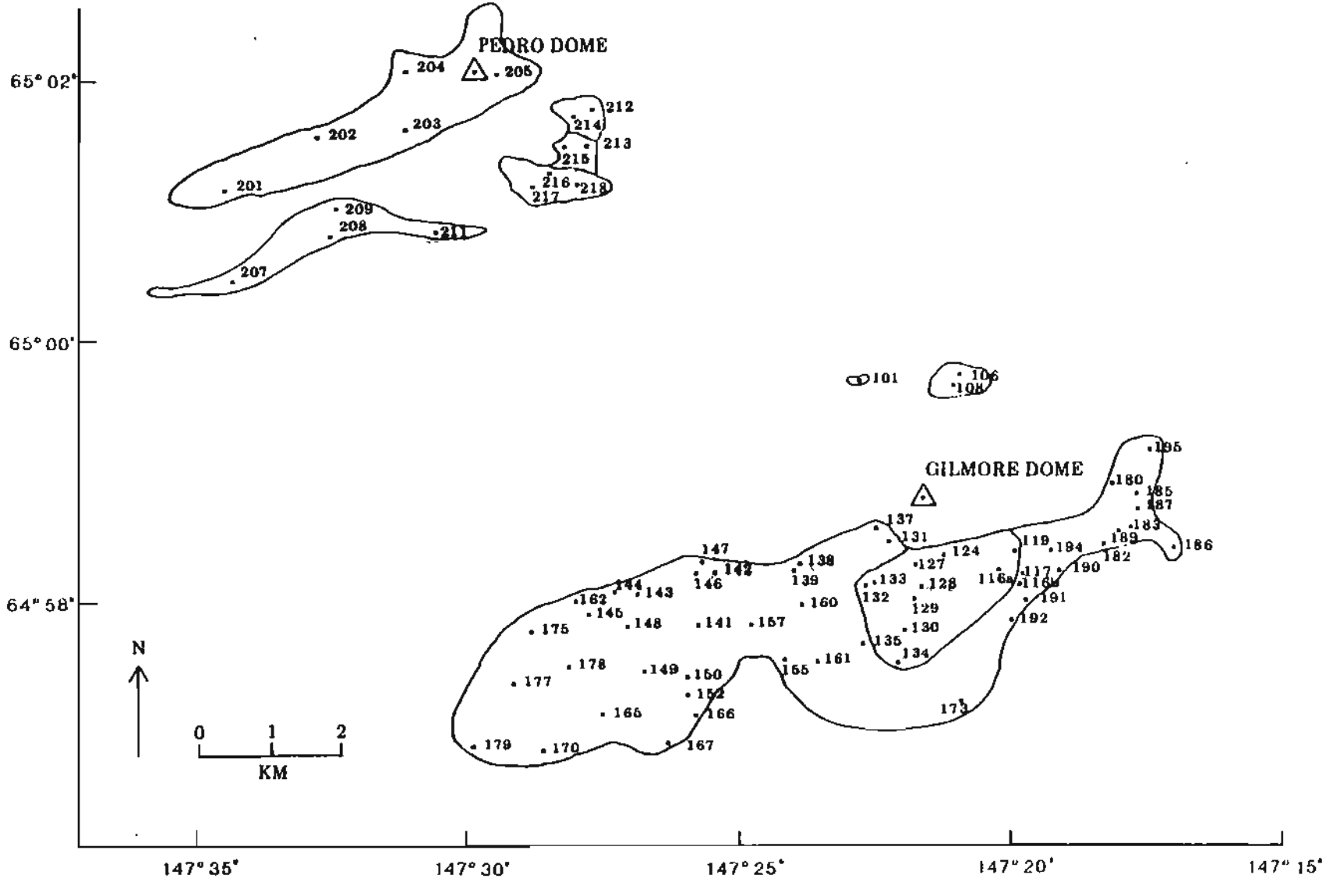

Figure 2. Distribution of sample locations, Gilmore Dome and Pedro Dome plutons, Fairbanks mining district, Alaska.

outcrops that are of greater magnitude than the within-outcrop variation can be considered significant. One large, easily accessible, porphyritic quartz monzonite rubble crop was chosen for a within-outcrop variation study. Eight samples were collected at equal spacings across a 9-m by 4-m rubble block. Stained slabs were prepared for each sample and were point-counted with a 400-point, 8-mm-spacing grid overlay. The results are listed in appendix C. The maximum within-outcrop modal variation for each mineral phase is less than the standard deviation calculated by the method of Van Der Plas and Tobi (1965) for each mineral phase. In conclusion, the within-outcrop variation study tends to support the assumption that the variability of one slab collected at each sample station is within the standard deviation of the analytical method. Variations that are of greater magnitude are presumably due to real differences among outcrops.

Grain-size Approximations

Ranges in grain size and average grain size for each major mineral in each intrusive phase were visually estimated. Range in grain size was measured and a 'best guess' at average grain size was determined for each sample. For the porphyritic granodiorite and porphyritic quartz monzonite, the estimations were determined on the stained slabs using a scale. For the fine-grained granodiorite and aplitic rocks, the estimations were determined in thin section based on a known field-of-view diameter for each objective power. It is stressed that the grain size estimates are semi-quantative and are included only for purposes of comparison among phases. The values for 'average' grain size have no statistical significance and are used in a general descriptive sense.

Trace-element and Major-oxide Analyses

Sixteen samples were analyzed for the trace elements rubidium and strontium. Analyses was done by X-ray fluorescence spectrometry by Bondar-Clegg and Company, Ltd., North Vancouver, British Columbia.

Forty-six samples were submitted for major-oxide analysis to the DGGS Minerals Laboratory. Ten major oxides were identified using X-ray fluorescence spectrometry of fused rock pellets, and FeO was determined by volumetric chemical analysis. The X-ray fluorescence spectrometer was calibrated using a combination of 19 Canadian and American whole-rock standards. Hutton and Elliot (1980) discuss the relative standard error associated with the X-ray fluorescence technique.

Rubidium and Strontium Isotopes

Rubidium-isotope and strontium-isotope analyses were done by Teledyne Isotopes of Westwood, New Jersey. Rubidium and strontium concentrations were measured by X-ray fluorescence spectrometry; $^{87}Rb/^{86}Sr$ ratios were calculated from these values using recommended isotope-abundance ratios. Strontium isotopic compositions were measured on a solid-source mass spectrometer. All analytical instruments were calibrated using nationally recognized standards.

GILMORE DOME PLUTONS

Porphyritic Granodiorite

Porphyritic granodiorite is restricted to a 5-km^2 area in the north central portion of the 30-km^2 Gilmore Dome pluton just south of Gilmore Dome, and to a small 1/2-km^2 pluton just north of Gilmore Dome (fig. 3). The rock is fine- to medium-grained hypidiomorphic-granular with coarse-grained megacrysts of quartz and potassium feldspar that constitute about 10 percent of the total rock. Major mineral constituents are plagioclase, quartz, and potassium feldspar. Biotite is the dominant mafic mineral, with lesser amounts of hornblende. Minor amounts of primary white mica, sphene, zircon, apatite, rutile, and opaques are also present. Although xenoliths are absent in the main Gilmore Dome pluton, they are abundant---and up to 1 m in diameter ---in the small pluton to the north. These xenoliths are dark colored and fine grained, with igneous-appearing textures. They represent either a more mafic intrusive phase carried from below by the magma, or a metamorphic inclusion that has re-equilibrated with the magma. Fresh surfaces of the porphyritic grandiorite are gray and weathered surfaces are dark gray to brown. A 1- to 4-cm-thick weathering rind is usually present on rubble blocks.

Porphyritic Quartz Monzonite

Porphyritic quartz monzonite comprises approximately 25 km^2 of the 30 km^2 Gilmore Dome pluton (fig. 3). The rock is medium-grained hypidiomorphic-granular; coarse-grained megacrysts of potassium feldspar and quartz comprise about one-third of the total rock. Although the mineral constituents and color are the same as those of the porphyritic granodiorite, the texture is more coarse, and the percentage of plagioclase relative to potassium feldspar is lower in the granodiorite. At sample locality 147---on the northern contact of the pluton---a rubble piece that represents the intrusive contact with either the country rock or a large xenolith was found. The contact is sharp and the foreign rock is not sheared. A planar foliation (schlieren) of about 50 percent biotite parallels the contact in the granitic rock. The foliation comes within 2 to 6 cm of the contact, and pinches and swells from 1 to 7 cm in width.

Aplite-pegmatite Dikes

Aplite-pegmatite dikes are found in both porphyritic rock types, but are far more common in the quartz monzonite. The dikes usually occur near the edge of the pluton and vary in width from 2 to 20 cm. One large 1/2-km^2 area is composed entirely of large aplite-pegmatite rubble, but lack of exposure of contacts makes it impossible to determine if this is a series of large dikes or a pluton of aplite-pegmatite material. The rock is white to light gray and contains fine-grained allotriomorphic-granular potassium feldspar, quartz, and plagioclase with up to 2 percent pink garnet or biotite, up to 1 percent primary white mica, and trace amounts of sphene. Within the fine-grained aplite dikes are layers and pods of coarse to very coarse grained pegmatitic potassium feldspar, quartz, and minor primary white mica.

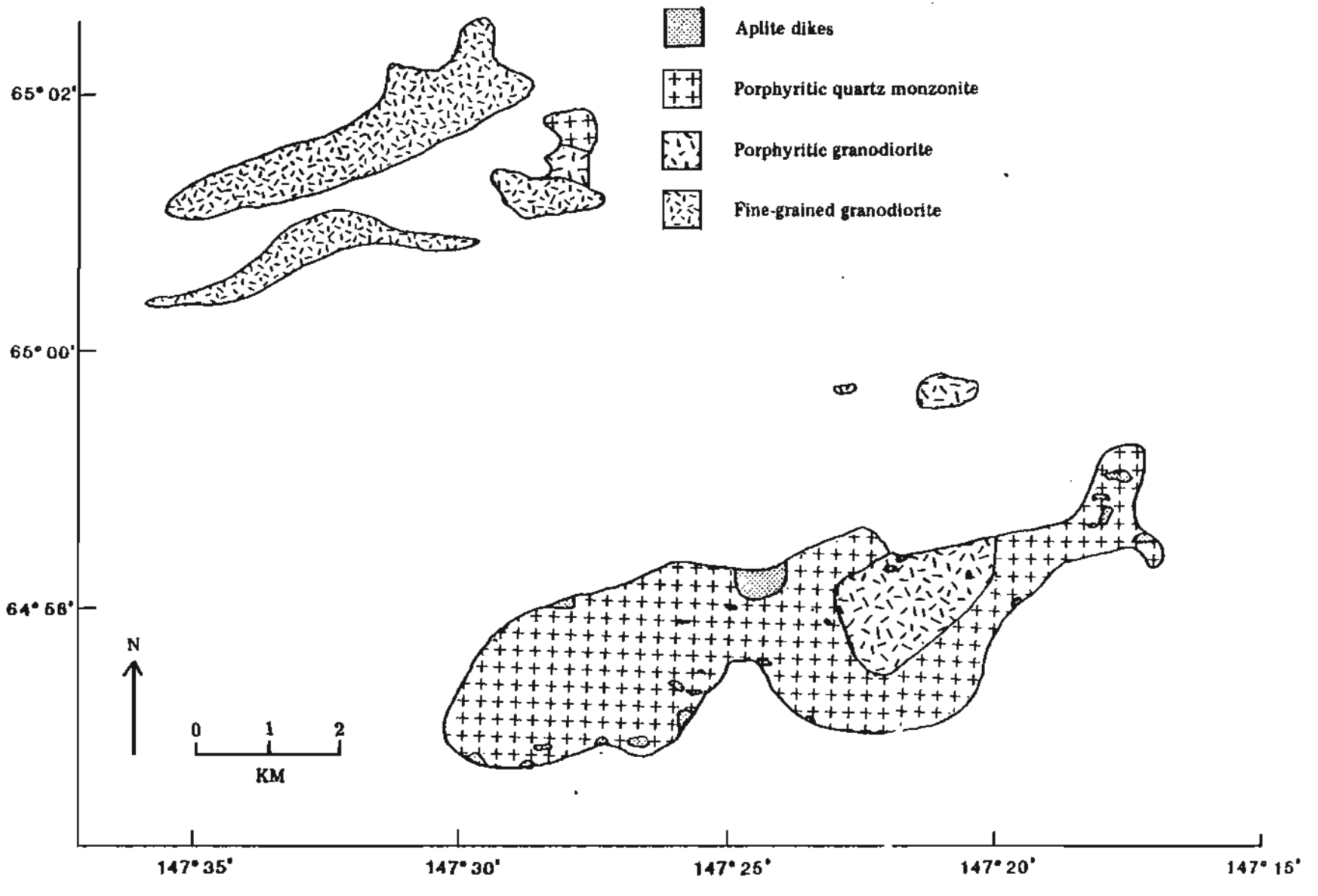

Figure 3. Distribution of rock types, Gilmore Dome and Pedro Dome plutons, Fairbanks mining district, Alaska.

Pyritic Aplite Bodies

Pyritic aplite bodies intrude the porphyritic quartz monzonite and nearby wall rock. The lack of exposure prevented determination of contact relationships between pyritic aplite bodies and other rocks. Presumably the pyritic aplite rocks, which are fine grained allotriomorphic-granular and consist of potassium feldspar, quartz, and plagioclase with up to 3 percent white mica and up to 1 percent pyrite, were intruded as large dikes or small plutons. The pyritic aplite is usually bleached white with zones and pods of reddish-brown stain caused by the oxidation of pyrite.

Coarse-grained Dikes

Two coarse-grained dikes (3 and 10 cm wide, respectively) were observed within the porphyritic quartz monzonite (sample locality 183). The larger dike is coarse- to medium-grained and composed of about 75 percent plagioclase, 20 percent quartz, and 5 percent primary white mica. Reddish-brown alteration products are present.

PEDRO DOME PLUTONS

Fine-grained Granodiorite

Fine-grained granodiorite is the dominant rock type in the Pedro Dome plutons, and comprises about 8.25 km^2 of the approximately 9 km^2 total area of intrusive rock. The fine-grained granodiorite plutons are exposed in three separate, elongate bodies (fig. 3). The largest pluton extends from Pedro Dome southwest about 5 km and covers an area of about 5 km^2. A second elongate pluton is exposed 1 km south of the first and trends southwest for about 4 km, covering an area of about 2.5 km^2. The third pluton crops out along the Steese Highway about 4 km southwest of Pedro Dome and covers an area of about 0.75 km^2. The rock is fine to medium grained hypidiomorphic-granular with a granodiorite composition that grades into quartz diorite in one area. The rock consists primarily of equigranular grains of plagioclase, quartz, biotite, hornblende, and lesser amounts of potassium feldspar. Minor amounts of augite, hypersthene, sphene, zircon, apatite, rutile, and opaques are also present. Small mafic xenoliths up to 1 cm in diameter are occasionally present in each of the three plutons. Larger mafic xenoliths up to 30 cm in diameter are abundant in the small pluton that crops out along the Steese Highway. Some xenoliths have igneous textures while others display a metamorphic foliation. Fresh surfaces of the fine-grained granodiorite are dark gray, while weathered surfaces are very dark gray to brown. A narrow 2- to 5-mm-thick weathering rind is often present on rubble blocks.

Porphyritic Granodiorite and Quartz Monzonite

Porphyritic granodiorite and quartz monzonite are restricted to one small 0.75-km^2 pluton about 3 km southeast of Pedro Dome (fig. 3). The southern portion of the pluton is predominantly granodiorite, while the northern portion is predominantly quartz monzonite. Due to lack of outcrop, the boundary between the two rock types and the relative proportion of the two rock types in the 0.75-km^2 pluton is uncertain. Narrow dikes of porphyritic

granodiorite up to 50 cm thick intrude the fine-grained granodiorite pluton near its contact with the porphyritic granodiorite pluton. Chilled borders are absent at all intrusive contacts.

Small aplite dikes with pegmatite pods and layers are present in the porphyritic rocks. Texturally and mineralogically, the porphyritic quartz monzonite and porphyritic granodiorite at Pedro Dome are identical to the equivalent rocks on Gilmore Dome. For this reason, as well as similar modal volumes and whole-rock chemistry, they are included with the equivalent rocks at Gilmore Dome in all subsequent discussions.

Altered Rock Bodies

Many small altered rock bodies are exposed in the Pedro Dome area. Grain size varies from fine to coarse, and the rocks are white with brown or red staining. Feldspars are usually altered to a combination of white mica, carbonate, clay, and epidote, which makes accurate identification of original rock types impossible. Coarse-grained stocks are probably altered quartz monzonites, while fine-grained stocks and dikes are probably either altered fine-grained granodiorite or aplite bodies.

MODAL VARIATION

Modal-volume data for 79 rock slabs are listed in appendix D. Figure 4 is a triangular diagram of modal quartz, potassium feldspar, and plagioclase. Rock names are based on a classification system developed by Bateman (1961) for granitic rocks of the Sierra Nevada. Superimposed on the diagram (for comparison) is a line representing the apparent differentiation trend for 24 intrusive masses in the southern Sierra Nevada (Moore, 1963).

A fractionation pattern similar to those found in the Sierra Nevada plutons exists among the intrusive rocks of the Gilmore-Pedro area. As the intrusive rocks become more differentiated, their composition shifts from the lower right to the center of figure 4, reflecting a decrease in plagioclase and an increase in potassium feldspar and quartz. The fine-grained granodiorite is the least fractionated intrusive phase. The porphyritic granodiorite was next in the fractionation sequence, followed by the porphyritic quartz monzonite, and finally the most fractionated intrusive phase, the aplite dikes.

The number of samples collected from each intrusive phase in the Gilmore-Pedro area depends on the outcrop area, and a scatter of points is present as expected. However, a fairly continuous fractionation trend is maintained. Figure 5 is a triangular plot of modal percentages of quartz, total feldspar, and mafics. Although there is a great deal of overlap between the porphyritic granodiorite and porphyritic quartz monzonite, the expected trend of decreased mafic content with increased fractionation is apparent.

Variation of modal mineralogy within the pluton is shown on figures 6 and 7. Figure 6 is a contour map of the potassium-feldspar to plagioclase ratio for the various plutons, and figure 7 is a contour map of the mafics to total feldspar + quartz ratio. To avoid complications related to late stage

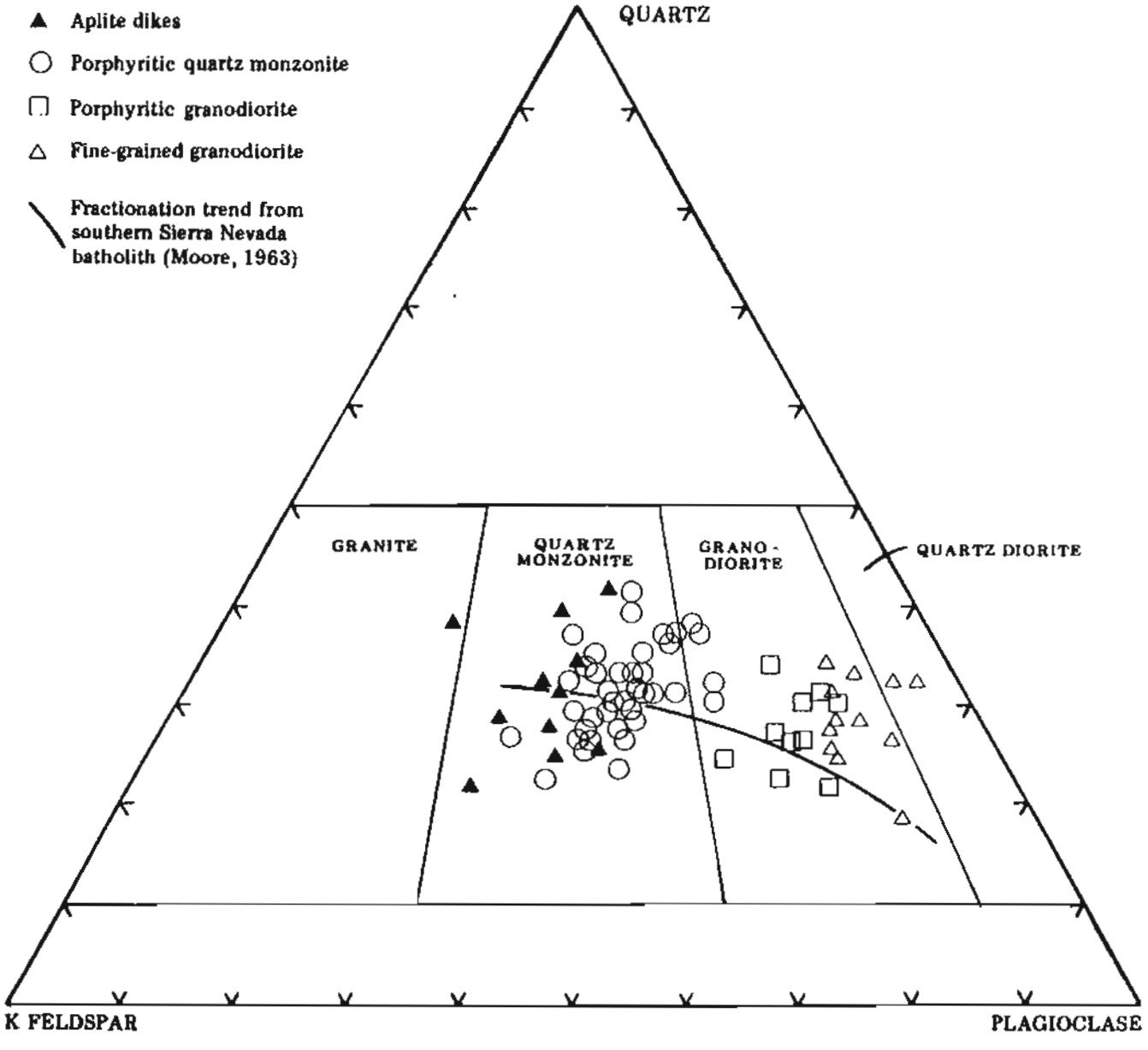

Figure 4. Quartz-potassium feldspar-plagioclase variation diagram.

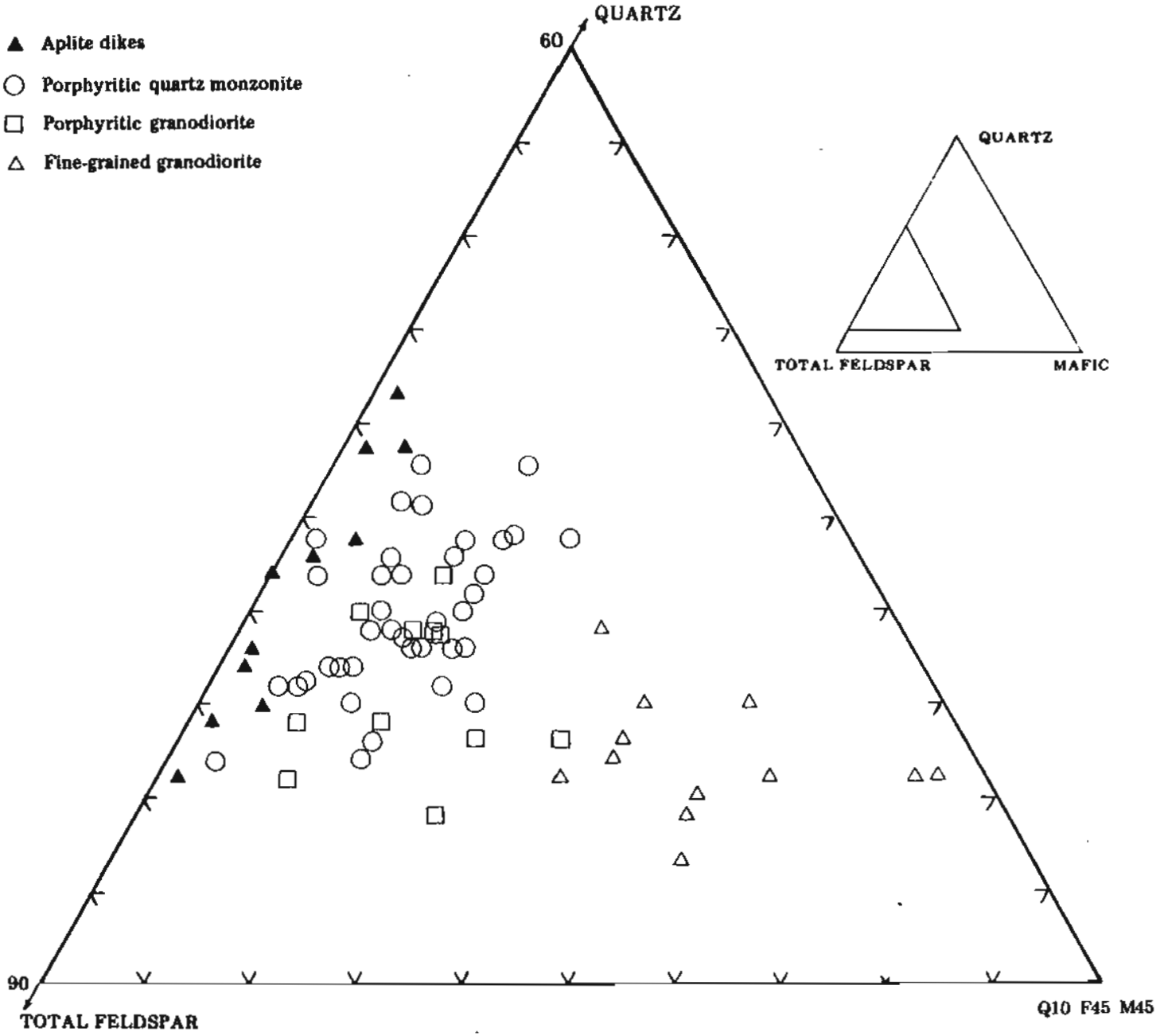

Figure 5. Quartz-total feldspar-mafic variation diagram.

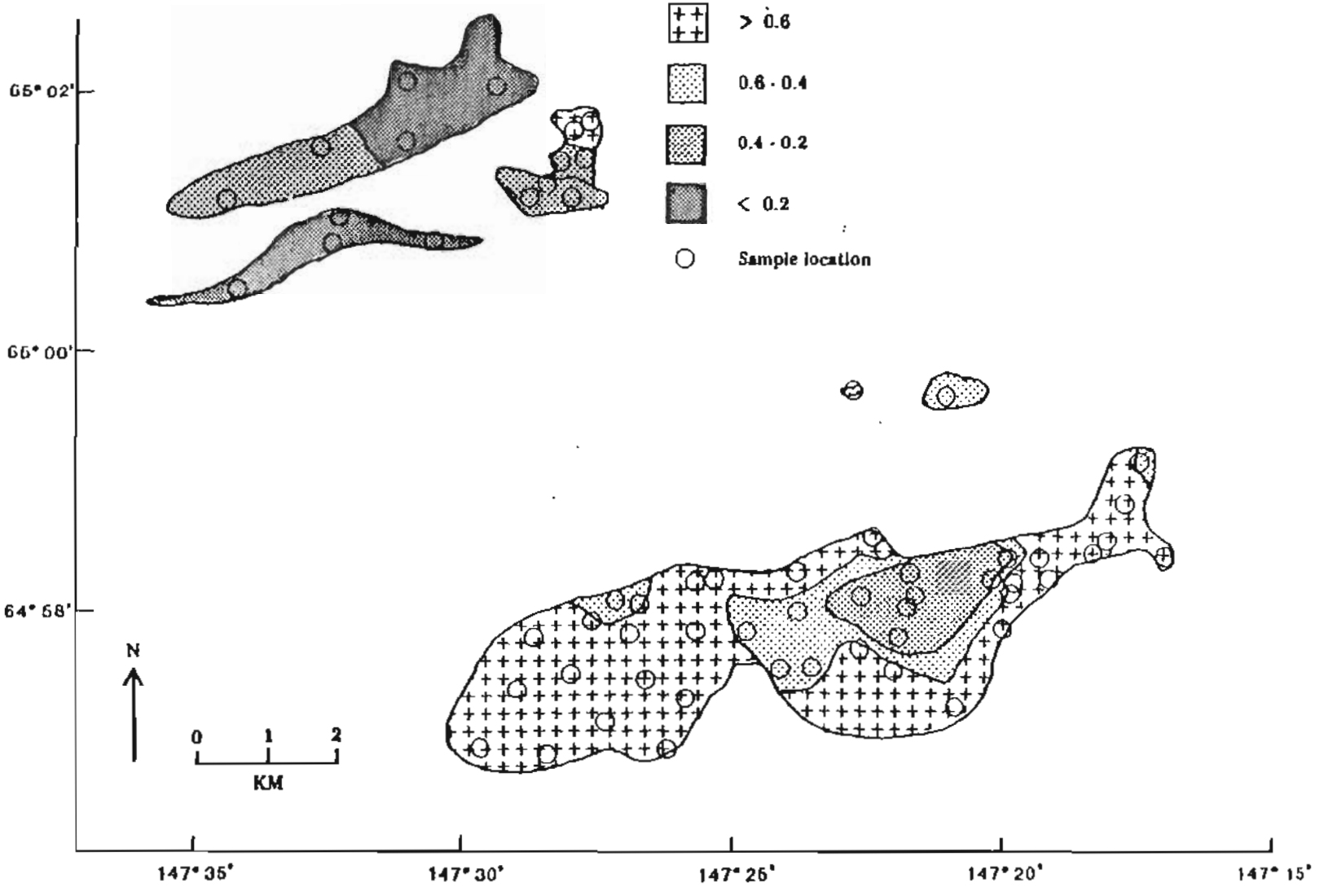

Figure 6. Distribution of the potassium-feldspar to plagioclase ratio.

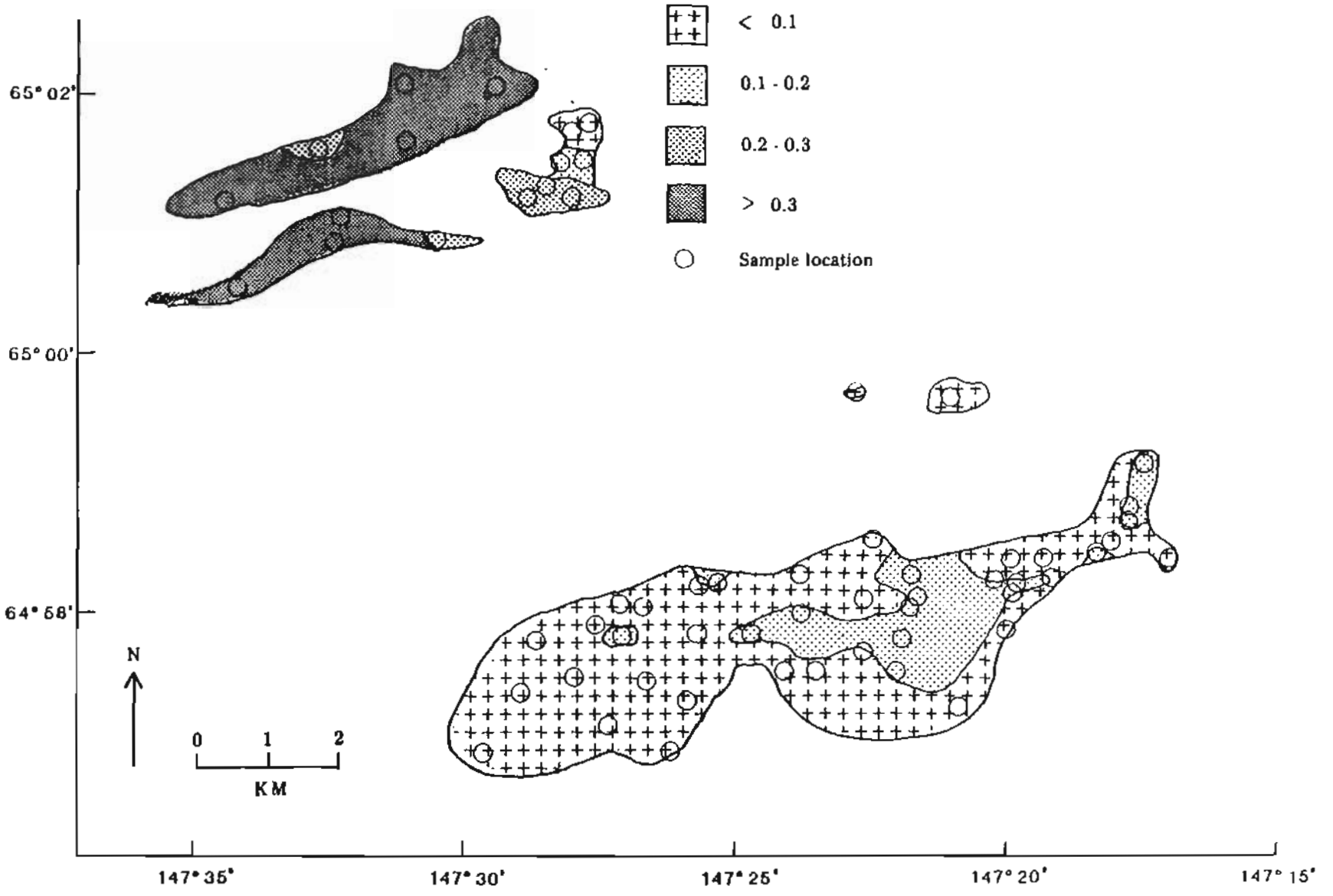

Figure 7. Distribution of the mafic to total feldspar + quartz ratio.

fractionation, the aplite samples are excluded. The obvious correlations between these maps and the map of the intrusive phases (fig. 3) is very apparent. Plagioclase and mafic minerals have high crystallization temperatures relative to potassium feldspar and quartz. Therefore, plagioclase and mafics are the first minerals to crystallize. With further fractionation, the abundance of plagioclase and mafics decreases and the abundance of potassium feldspar and quartz increases.

The pattern illustrated in figures 6 and 7 indicates that if fractional crystallization caused the modal variation among the plutons, the fine-grained granodiorite phase that forms the plutons at Pedro Dome was the first phase to crystallize, followed by the porphyritic granodiorite phase that forms two small plutons and the central portion of the Gilmore Dome pluton. The next magma to crystallize was the porphyritic quartz monzonite phase that forms one small pluton at Pedro Dome and the bulk of the Gilmore Dome pluton. The final phase to crystallize was the aplitic rocks that form dikes within the porphyritic rocks.

MINERALOGY

Plagioclase

Plagioclase is a major constituent in each intrusive phase. It is fine- to medium-grained in the fine-grained granodiorite and aplite dikes and fine- to coarse-grained in the porphyritic phases. There is a general decrease in modal percentage of plagioclase in progressively more differentiated phases (table 1) because of early crystallization and removal of plagioclase from the

Table 1. Modal percentage and grain size of plagioclase.

Intrusive phase	Modal percentage		Grain size (mm)	
	Range	Mean	Range	Average
Fine-grained granodiorite	39-51	45	0.2-2	1
Porphyritic granodiorite	44-54	49	1-5	2
Porphyritic quartz monzonite	30-43	36	1-7	3
Aplite dike	19-38	30	0.2-2	1

crystallizing magma. One deviation from this pattern is a slight increase in plagioclase (due to the much greater amount of hornblende) in the fine-grained granodiorite relative to the porphyritic granodiorite. Hornblende is also a high-temperature, early-formed mineral with many of the same constituents as plagioclase, especially calcium and aluminum. The contemporaneous crystallization of hornblende with plagioclase during the crystallization of

the fine-grained granodiorite apparently depleted the magma of constituents necessary to make plagioclase. This resulted in the slight deviation from decreased plagioclase content with increased fractionation.

Plagioclase crystals are generally subhedral to euhedral. Many grains in each phase display oscillatory extinction indicative of compositional zonation. Albite twinning is very common in the plagioclase grains of each phase. Albite-Carlsbad, Carlsbad, and pericline twinning are less common. Anorthite contents were determined from extinction angles of albite twins by the Michael-Levy method. The cores of zoned crystals have a higher anorthite content than the rims and unzoned crystals in each phase. Anorthite content in each phase generally varies by about 10 to 20 percent, with nearly total overlap between the intrusive phases. Anorthite content varies from An_{22} to An_{48}. Compositional zoning of individual crystals causes a variation in An content from 5 to 15 percent from the core to the rim of zoned crystals. This indicates that anorthite content decreased with increased fractionation as crystallization proceeded within each phase.

Plagioclase occasionally contains inclusions of quartz, biotite, apatite, hornblende, and pyroxene. Alteration of plagioclase is common and is most extensive in calcic cores and along cleavage directions. Alteration products include a combination of fine-grained white mica, carbonate, clay, and epidote.

Potassium Feldspar

Potassium feldspar occurs in moderate amounts in the granodiorites and as a major constituent in the quartz monzonites and aplite dikes. It is fine- to medium-grained in the fine-grained granodiorite and aplite dikes and medium- to coarse-grained in the porphyritic rocks (table 2). Generally, the amount of potassium feldspar increases with increased fractionation.

Table 2. Modal percentage and grain size of potassium feldspar.

	Modal percentage		Grain size (mm)	
Intrusive phase	Range	Mean	Range	Average
Fine-grained granodiorite	2-11	7	0.2-2	1
Porphyritic granodiorite	10-23	16	1-20	2
Porphyritic quartz monzonite	17-40	28	1-30	6
Aplite dike	25-54	38	0.2-4	1

Potassium feldspar crystals are generally anhedral to subhedral with additional euhedral to subhedral megacrysts in the porphyritic rocks. Both

the size and abundance of megacrysts vary with degree of fractionation among the various phases. The least fractionated phase (fine-grained granodiorite) contains no potassium feldspar megacrysts. The porphyritic granodiorite contains about 5 percent potassium feldspar megacrysts with a maximum size of 20 mm. The porphyritic quartz monzonite contains about 15 percent potassium feldspar megacrysts with a maximum size of 30 mm. Finally, the most fractionated phase, the aplites dikes, contain no potassium feldspar megacrysts. Bateman and Chappell (1979) point out that this pattern of megacryst distribution in calc-alkaline granitic suites is common, and cite many examples in which a) earliest and least differentiated rocks of a comagmatic granitic suite are equigranular, b) the next younger rocks contain megacrysts, and c) the most differentiated rocks are equigranular. This relationship is explained in the section on textural variation based on experimental work by Swanson (1977) dealing with crystal growth and nucleation in magmas of granite and granodiorite composition.

Carlsbad twinning of potassium feldspar is common in each phase. 'Grid-iron' twins with narrow streaky perthitic intergrowths are common in all but the fine-grained granodiorite phase. Graphic intergrowths of potassium feldspar with quartz are found along grain boundaries between quartz and potassium feldspar in each phase.

Potassium feldspar commonly contains inclusions of quartz, biotite, and plagioclase, and occasionally hornblende, sphene, apatite, and pyroxene. The arrangement of these crystals in zones parallel to crystal faces in potassium feldspar megacrysts shows stages in the growth of the megacrysts. The inclusions seem to have been pushed in front of and finally included in the advancing faces of the potassium feldspar crystals.

Minor alteration of potassium feldspar is present in all phases. Alteration products are a combination of fine-grained white mica, carbonate, and clay.

Quartz

Quartz is a major constituent in all intrusive phases. It is fine to medium grained in the fine-grained granodiorite and aplite dikes and fine to coarse grained in the porphyritic phases (table 3). The modal percentage of

Table 3. Modal percentage and grain size of quartz.

	Modal percentage		Grain size (mm)	
Intrusive phase	Range	Mean	Range	Average
Fine-grained granodiorite	14-29	22	0.2-2	1
Porphyritic granodiorite	19-32	26	1-10	2
Porphyritic quartz monzonite	22-38	30	1-12	5
Aplite dike	21-42	31	0.2-4	2

quartz increases with increased differentiation in a manner similar to potassium feldspar. The size and distribution of quartz megacrysts are also similar to potassium feldspar.

Quartz crystals are generally anhedral with some subhedral to euhedral megacrysts in the porphyritic rocks. Megacrysts up to 10 mm long make up about 5 percent of the porphyritic granodiorite, while megacrysts up to 12 mm long make up about 10 percent of the porphyritic quartz monzonite. These megacrysts have a hexagonal-trapezohedral crystal form that indicates they are psuedomorphs after high-temperature beta quartz.

Some quartz grains display strained extinction. Inclusions are very common and include plagioclase, biotite, and occasionally hornblende, sphene, and pyroxene. Quartz veinlets from 1 to 5 mm wide occur occasionally in each phase.

Biotite

Biotite occurs in minor amounts in all phases, and is the dominant mafic mineral in all phases except the fine-grained granodiorite, which has nearly equal amounts of hornblende. Biotite is fine to medium grained in the intrusive rocks (table 4). The modal percentage of biotite decreases with increased differentiation in a pattern similar to that of plagioclase, probably because of the high crystallization temperature of both minerals.

Table 4. Modal percentage and grain size of biotite.

Intrusive phase	Modal percentage		Grain size (mm)	
	Range	Mean	Range	Average
Fine-grained granodiorite	8-21	13	0.2-1	0.5
Porphyritic granodiorite	2-17	8	1-4	1
Porphyritic quartz monzonite	1-13	7	1-7	2
Aplite dike	0-2	1	0.1-1	0.5

Biotite crystals are generally subhedral with strong pleochroism. Optically, X is light brown and Y and Z are dark brown. Biotite contains inclusions of zircon (with well-developed pleochroic halos), quartz, opaques, rutile, and occasionally sphene and hornblende.

Biotite alters to chlorite (penninite), from trace amounts up to 30 percent of the total biotite. Biotite is occasionally altered to epidote, and also forms reaction rims around, and in some cases totally replaces hornblende and pyroxene.

Hornblende

Hornblende is not found in the aplitic rocks, occurs in minor to trace amounts in the porphyritic rocks, and is the dominant mafic mineral in the leucocratic, fine-grained granodiorite. It is fine- to medium-grained in each intrusive phase in which it is found. Hornblende has a high crystallization temperature, and therefore its abundance tends to decrease with increased fractionation in a manner similar to biotite and plagioclase (table 5).

Table 5. Modal percentage and grain size of hornblende.

Intrusive phase	Modal percentage		Grain size (mm)	
	Range	Mean	Range	Average
Fine-grained granodiorite	6-20	11	0.1-1	0.5
Porphyritic granodiorite	0-4	1	0.1-2	1
Porphyritic quartz monzonite	0-3	0	0.5-4	1
Aplite dike	0	0	0	0

Hornblende crystals are subhedral to euhedral and have strong pleochroism. Optically, X is colorless to yellow, Y is pale green to greenish brown, and Z is green to dark olive or blue green. Hornblende contains inclusions of quartz and opaques. Some grains are twinned on the (100) plane.

Hornblende is sometimes partially altered to epidote and white mica, and also forms reaction rims on, and sometimes totally replaces pyroxene crystals. Biotite and white mica commonly form reaction rims on, and sometimes replace hornblende grains.

Pyroxene

Pyroxene occurs only in the fine-grained granodiorite intrusive phase. Of the 12 thin-sections examined from this phase, three have trace amounts of augite, and one has 8 percent augite plus a trace of hypersthene. Pyroxene grains are typically subhedral and fine-grained.

The augite is colorless, has an extinction angle of 44° to 51°, and has a medium 2V angle. It is often polysynthetically twinned and displays twin seams. Hypersthene is distinctly pleochroic. Optically, X is pink, Y is pale brown, and Z is pale green. The hypersthene has parallel extinction and is not twinned.

Hypersthene crystallized earlier than augite. When it later reacted to form augite, small cores of hypersthene remained in some augite grains. Britton (1970) reports up to 5 percent hypersthene in some fine-grained

granodiorites from Pedro Dome. In these rocks, the reaction of hypersthene to form augite is not well developed. Augite is usually mantled by hornblende reaction rims and is occasionally mantled by biotite reaction rims. Pyroxene crystals tend to form mafic clusters with hornblende.

White Mica

Primary white mica does not occur in the fine-grained granodiorite. It occurs in most samples of porphyritic rock up to a maximum modal volume of 1 percent. All but one of the 13 aplitic rock samples contain primary white mica with a maximum modal volume of 3 percent.

White mica is fine-grained, and in the porphyritic rocks it is often in contact with biotite grains. In one rare coarse-grained dike rock, primary white mica is medium grained and makes up about 5 percent of the rock.

Accessory Minerals

Sphene is the most common accessory mineral. It is found as euhedral crystals and subhedral crystal fragments. Sphene occurs uncommonly in trace amounts in aplitic rocks, commonly in trace amounts in fine-grained granodiorite and porphyritic quartz monzonite, and in amounts up to 1 percent in porphyritic granodiorite. Sphene crystals sometimes contain inclusions of quartz. Trace amounts of opaques, apatite, zircon, and rutile are found in each rock type.

Pink garnet comprises up to 2 percent of many of the aplite-pegmatite dikes. The sulfide-rich aplitic rocks contain from trace amounts to 1 percent sulfide minerals. Studies of polished sections in reflected light show the sulfide is pyrite. The sulfide-rich aplitic rocks are usually stained brownish red from sulfide oxidation.

TEXTURAL VARIATION

Many large plutons display concentric textural and compositional variations very similar to those variations seen between the various plutons in the Gilmore-Pedro area. Textural variation within the concentrically zoned plutons is often attributed to loss of heat to the surrounding wall rock. It has been suggested that because temperatures fall more rapidly in the marginal regions of a pluton than in the interior, fine-grained marginal rocks are fine-grained and interior rocks are more coarse-grained (Bateman and Chappell, 1979).

The Gilmore-Pedro plutons do not display this type of within-pluton concentric zoning, and there is no observable change in igneous textures related to distance from the contacts. Yet the entire range of textural variation in concentrically zoned plutons exists among the plutons of the Gilmore-Pedro fractionation suite. The textural variation is dependent on a factor that is independent of position within a given pluton. Recent experimental investigations of granitic textures offer an explanation of textural relationships that is independent of the theory of varied heat loss to wall rocks.

Experimental investigations by Swanson (1977) show that in synthetic granite and granodiorite magma, the crystal growth rate reaches a maximum at very low undercoolings and drops off considerably at higher undercoolings at 8 kbar pressure. Nucleation density, however, is a minimum at low undercoolings and reaches a maximum at relatively high undercoolings. Therefore, at low undercoolings, there is a low nucleation density coupled with rapid crystal growth, while at high undercoolings there is a high nucleation density accompanied by slow crystal growth.

This experimental relationship may help explain the size and distribution of potassium feldspar and quartz megacrysts as well as overall grain size in various phases of the Gilmore-Pedro fractionation suite. Although crystallization behavior in synthetic systems has useful applications for explaining textures in natural systems, it must be stressed that these systems have important differences. Crystallization experiments use a single bulk composition, water content, and pressure. Bulk composition, water content, and pressure can all change during the intrusion and crystallization of a natural magma. The synthetic system is a gross oversimplification of a natural system, and comparisons should be made with caution. It is valid, however, to use the experimentally determined relationship between undercooling and crystal nucleation and growth rate in a qualitative sense to study the development of igneous textures in a natural system such as the Gilmore-Pedro fractionation suite. With this in mind, the experimentally determined relationships will be used to create a simplified scenario for the crystallization and development of various textures found in the Gilmore-Pedro plutons.

The liquidus temperature of the least differentiated, fine-grained granodiorite phase will be the highest of all the intrusive rock phases because of its high-temperature mineral assemblage. The liquidus temperature of the magma should decrease with fractionation. When the fine-grained granodiorite magma rose to a region of lower confining pressure and intruded the cooler country rock, it began to crystallize. Because of its high liquidus temperature and cool surrounding rock, crystallization took place at a relatively high undercooling. These conditions correspond to a high nucleation rate and low crystal growth rate that resulted in a fine-grained rock devoid of megacrysts. The porphyritic granodiorite has a slightly lower liquidus temperature, which resulted in a smaller undercooling and intermediate nucleation and crystal growth rate. This resulted in a medium-grained rock with only a small amount of moderately sized megacrysts. The porphyritic quartz monzonite phase has an even lower liquidus temperature, much closer to the temperature of the country rock. This resulted in a relatively low undercooling, which corresponds to a low nucleation rate and high crystal growth rate. This explains the coarser overall grain size and high percentage of large potassium feldspar and quartz megacrysts in the porphyritic quartz monzonite.

The first three phases to crystallize (fine-grained granodiorite, porphyritic granodiorite, and porphyritic quartz monzonite) did so under conditions whereby water pressure did not exceed lithostatic pressure. However, during fractionation, water was concentrated in the residual melt until water pressure finally exceeding lithostatic pressure. At this time,

the previously crystallized porphyritic granodiorite and porphyritic quartz monzonite and intruded as aplite dikes or small plutons. This sudden decrease in P_{water} caused the liquidus temperature to increase, which resulted in increased undercooling. This increase in undercooling promoted a high nucleation density with low crystal growth rate, which explains the fine-grained texture and lack of megacrysts in the aplitic phase.

Swanson (1977) determined experimentally that porphyritic textures do not require a two-stage crystallization history whereby megacrysts are crystallized early and carried with the magma to a new environment where the finer grained ground mass rapidly crystallizes. Instead, porphyritic textures can be produced during one-step crystallization where larger grains of a faster-growing phase grow simultaneously with or after small grains of a more slowly growing phase.

This appears to be the case with the crystallization of the porphyritic rocks of the Gilmore-Pedro fractionation suite. Large potassium feldspar and quartz megacrysts crystallized rapidly after the finer grained, higher temperature phases crystallized. The megacrysts included the fine-grained crystals in zones parallel to their crystal faces, showing the stages in the growth of the megacrysts.

WHOLE-ROCK CHEMISTRY

Rock samples from each intrusive body were analyzed for several trace-elements and major oxides to determine chemical composition and variation within each rock type and as a further test of whether the various intrusive phases were comagmatic or derived from several parent magmas.

Trace Elements

The trace elements rubidium and strontium were analyzed as a possible measure of the degree of fractional crystallization. Neither rubidium nor strontium are a major constituent of the rock-forming minerals and therefore act as a dispersed trace element in igneous rocks. The distribution of rubidium is dependent on the similarity of the radius of the Rb^{+} ion (1.48 Å) to the K^{+} ion (1.33 Å) (Faure and Powell, 1972). Rubidium substitutes for potassium in all rock-forming minerals that contain potassium, for example the micas and in particular, potassium feldspar. The distribution of strontium in rocks is controlled by the substitution of Sr^{2+} (radius = 1.13 Å) for Ca^{2+} (radius = 0.99 Å) (Faure and Powell, 1972) in calcium-bearing minerals such as apatite and especially plagioclase. The Sr^{2+} ion is too large, however, to substitute for Ca^{2+} in six-fold coordinated lattice positions such as those in pyroxenes. Potassium feldspar can also contain Sr^{2+} ions in place of K^{+} ions. During fractional crystallization of a magma, strontium is initially removed from the melt phase and concentrated in calcic plagioclase, while rubidium is concentrated in the residual fluid. Therefore, the rubidium-strontium ratio of comagmatic igneous rocks tends to increase with increased differentiation caused by both an increase in rubidium and a decrease in strontium.

Sixteen samples which represented each of the intrusive phases were analyzed for rubidium and strontium. Rubidium concentrations range from 76 to 244 ppm in granodiorites and quartz monzonite, with values up to 390 ppm in aplite dikes. Strontium concentrations range from 285 to 690 ppm in granodiorites and quartz monzonite with values down to 34 ppm in aplite dikes. Data are listed in appendix E.

A useful method of illustrating the enrichment of rubidium relative to strontium in a differentiating magma is to plot rubidium versus rubidium-strontium ratio. This relationship is shown using a semi-log scale in figure 8. A coherent, nearly linear fractionation trend is apparent on figure 8. The fine-grained granodiorite samples have the least rubidium and are the least fractionated of all the samples. The porphyritic granodiorite samples have slightly more rubidium and are more fractionated. The porphyritic quartz monzonite samples have even more rubidium and are more fractionated still. The aplite-dike samples contain the greatest amount of rubidium and represent the most highly fractionated rocks.

Major Oxides

Forty-six intrusive rock samples were analyzed for major oxides. Sample locations were chosen to be as evenly distributed within the plutons as sample freshness would permit. Therefore, the number of major-oxide analyses from each intrusive phase is dependent on the outcrop area of each phase. Of 46 analyses listed in appendix F, 24 are porphyritic quartz monzonite, 10 are porphyritic granodiorite, seven are fine-grained granodiorite, and five are aplite dikes.

Major-oxide data are plotted in figure 9 on a Harker variation diagram. The wide range of SiO_2 content---from 59 to 78 percent---is apparent on the Harker diagram. Smooth, continuous trends are observed for the variation of each major oxide with SiO_2. FeO (total), MgO, CaO, and Al_2O_3 decrease with increased SiO_2, while K_2O and Na_2O increase with increased SiO_2. At high SiO_2 contents, several points on the CaO and Al_2SiO_3 plots do not fall on the main trend. The three points that fall below the CaO trend are aplite dikes, and their depletion in CaO is probably caused by the low plagioclase content of these highly fractionated rocks. The scatter of the Al_2O_3 trend is fairly random and probably represents depletion of aluminum due to weathering rather than crystal accumulation of plagioclase. Smooth patterns such as those on the Harker diagram are often attributed to the evolution of the composition of the residual magma during fractional crystallization---the liquid line of descent. The position of each intrusive phase in the evolution of the magma from early crystallization to late crystallization is clearly fine-grained granodiorite to porphyritic granodiorite to porphyritic quartz monzonite to aplite dikes.

Figure 10 is a plot of the Gilmore-Pedro samples on an AFM diagram. For purposes of comparison, whole-rock data from the well-studied Tuolumne intrusive suite (Bateman and Chappell, 1979) are also plotted. The Tuolumne intrusive suite is a concentrically zoned plutonic sequence that is part of the well-known central Sierra Nevada batholith in California. This particular intrusive suite was chosen for comparison because it is a thoroughly studied comagmatic plutonic sequence similar in composition to the Gilmore-Pedro

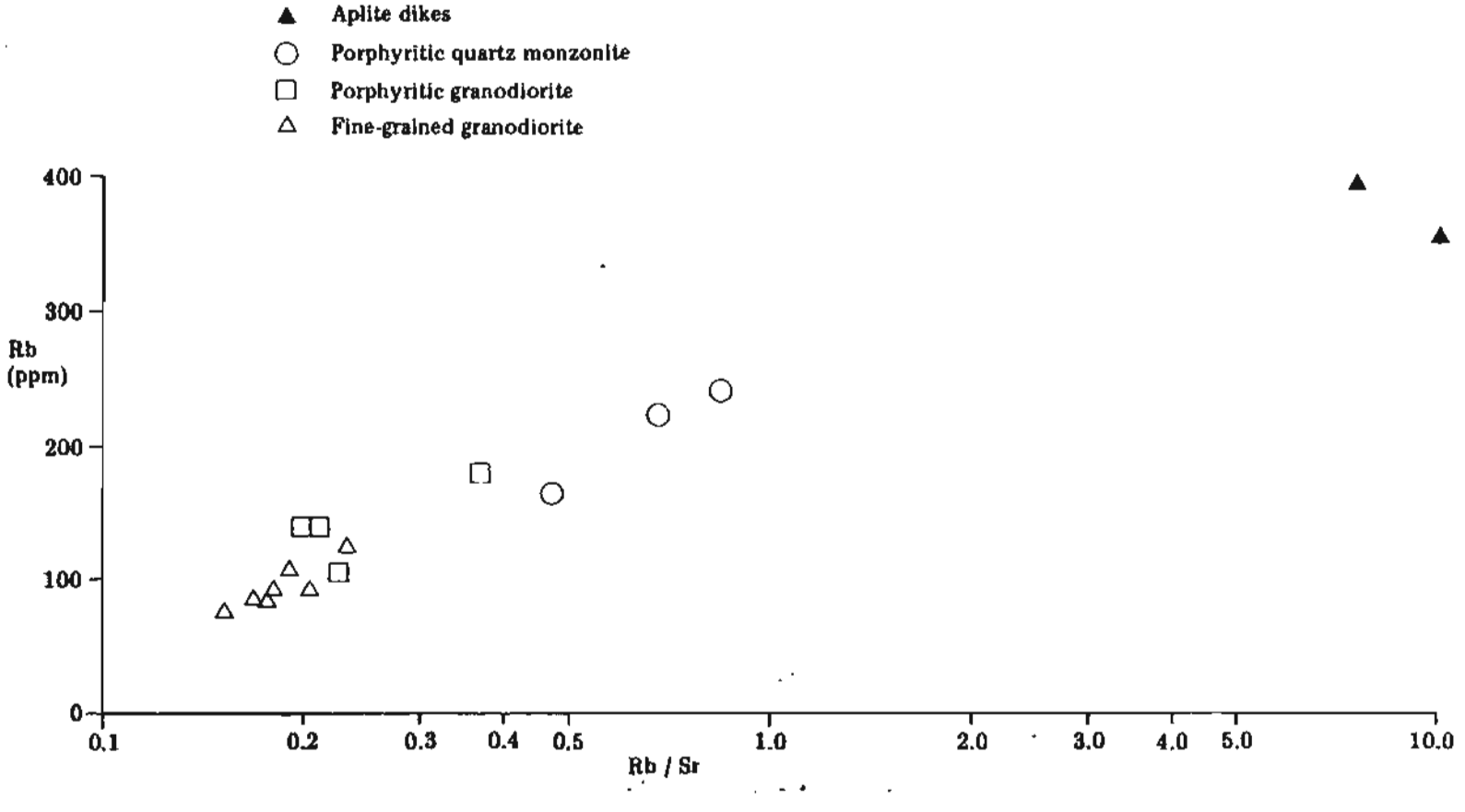

Figure 8. Rubidium-strontium variation diagram.

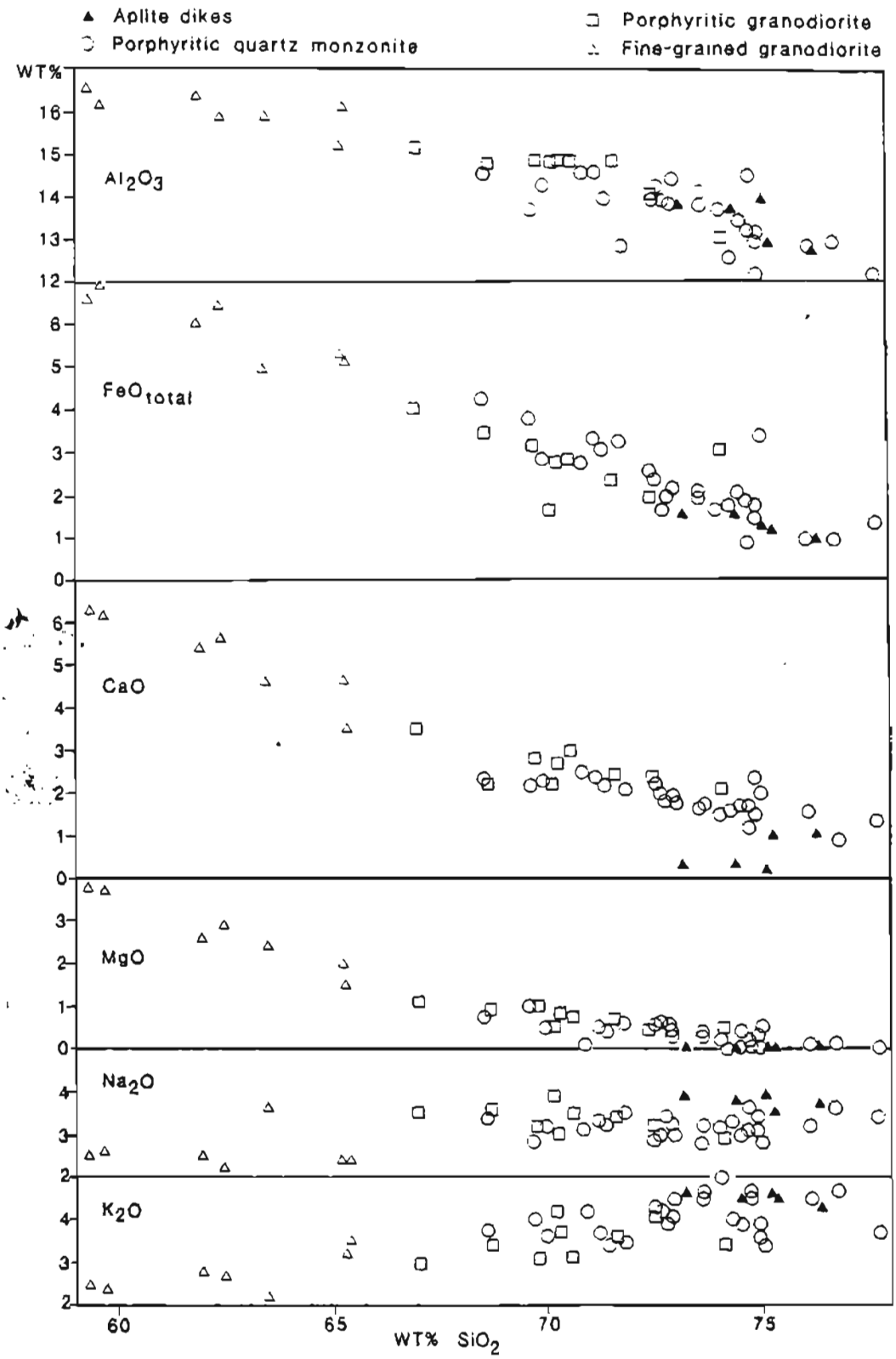

Figure 9. Major-oxide data plotted on Harker variation diagram.

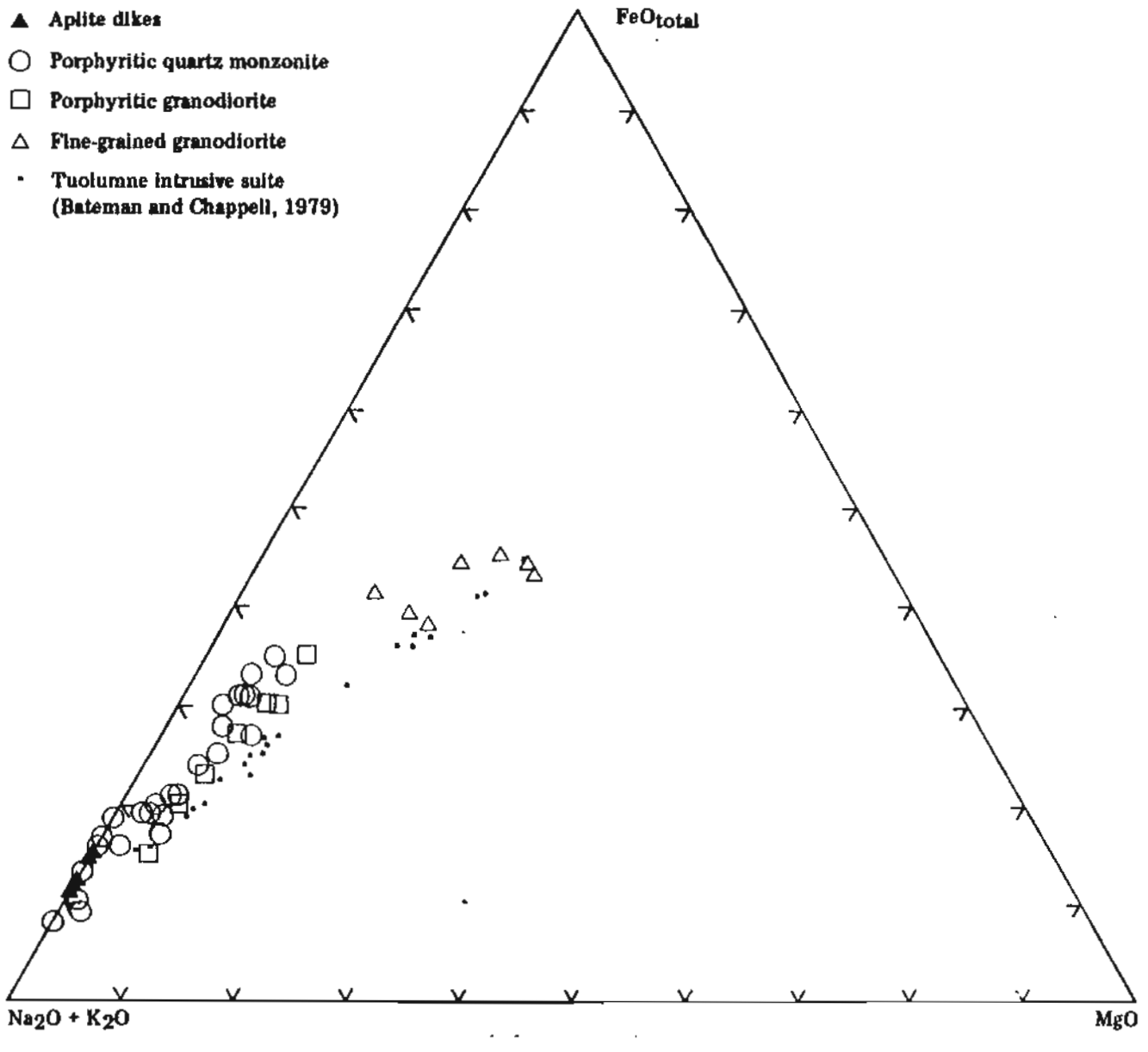

Figure 10. Plot of Gilmore Dome and Pedro Dome samples on an AFM diagram.

intrusive suite. The major-oxide whole-rock data from the Tuolumne suite are from a study by Bateman and Chappell (1979) that was undertaken to develop and test a model for the origin of comagmatic plutonic sequences in the Sierra Nevada. Two separate trends are apparent on figure 10. One trend is formed by the Tuolumne data and another by the Gilmore-Pedro data. These trends are typical of comagmatic calc-alkaline intrusive suites. As crystallization proceeded in both the Tuolumne and Gilmore-Pedro intrusive suites, the magmas became progressively enriched in alkalis relative to iron and magnesium. The fractionation progression as interpreted from the AFM diagram for the Gilmore-Pedro suite is (from least to most fractionated) fine-grained granodiorite, porphyritic granodiorite, porphyritic quartz monzonite, and aplite dikes.

Figure 11 is a Ca-Na-K diagram on which the Gilmore-Pedro samples are plotted. Enrichment in alkalis relative to calcium with progressive fractionation from fine-grained granodiorite to porphyritic granodiorite to porphyritic quartz monzonite to the aplite dikes is the observed pattern. Figures 12 and 13 are contour maps illustrating the spatial variation in the alkali to iron + magnesium ratio and the alkali to calcium ratio. These figures illustrate the spatial variation in composition of the intrusive rocks. The AFM and Ca-Na-K fractionation trends are very similar spatially to fractionation trends inferred from modal data (figs. 6 and 7). The least fractionated rocks are the fine-grained granodiorites that make up the three elongate plutons at Pedro Dome. The next most fractionated are the porphyritic granodiorites that form two small plutons and the central portion of the Gilmore Dome pluton. Still further in the fractionation of the magma are the porphyritic quartz monzonites that make up one small pluton and the bulk of the Gilmore Dome pluton. Finally, the most fractionated rocks are the aplite dikes that are not shown on the contoured diagram.

CIPW normative mineral contents for each whole-rock analysis are listed in appendix G. All samples (except the five fine-grained granodiorites) are corundum-normative and many have greater than 1 percent normative corundum. This fact, along with the presence of primary white mica, reflects the relatively high Al_2O_3 content of these rocks. Variations in normative quartz, feldspars, and mafics between the intrusive phases reflect the same patterns of chemical variation with fractionation illustrated on the major-oxide variation diagrams and modal-mineral-content diagrams.

Conclusion

Whole-rock chemical data are consistent with the fractionation model proposed from the modal-variation data and petrographic and field observations. The fractionation sequence began with the crystallization of fine-grained granodiorite followed by porphyritic granodiorite, porphyritic quartz monzonite, and finally the aplite dikes. As the fractionation proceeded, the weight percent of rubidium increased and strontium decreased, and the weight percent of the major oxides SiO_2, K_2O, and Na_2O increased while CaO, Al_2O_3, FeO (total), and MgO decreased.

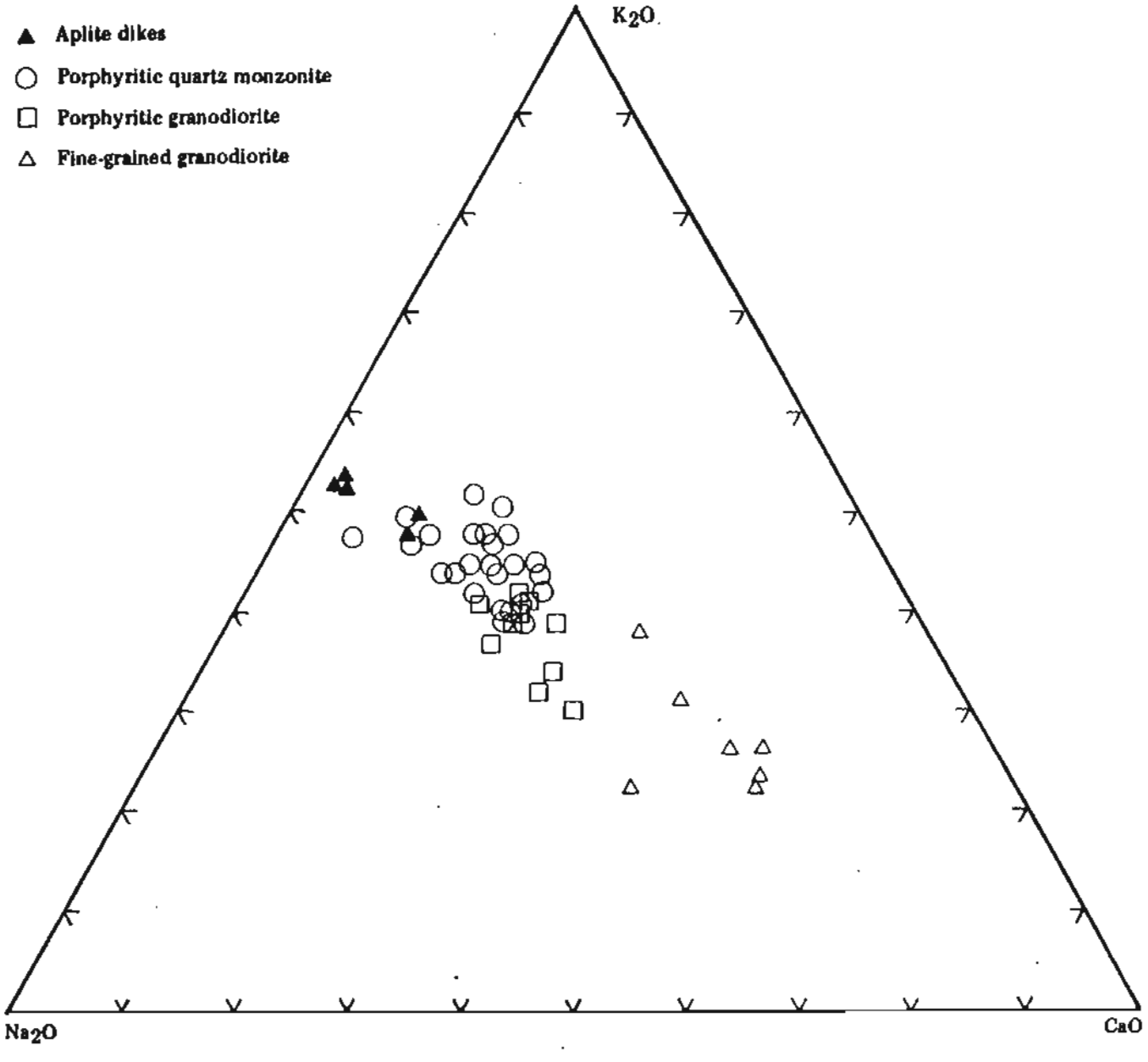

Figure 11. Plot of the Gilmore Dome and Pedro Dome samples on a Na-Ca-K diagram.

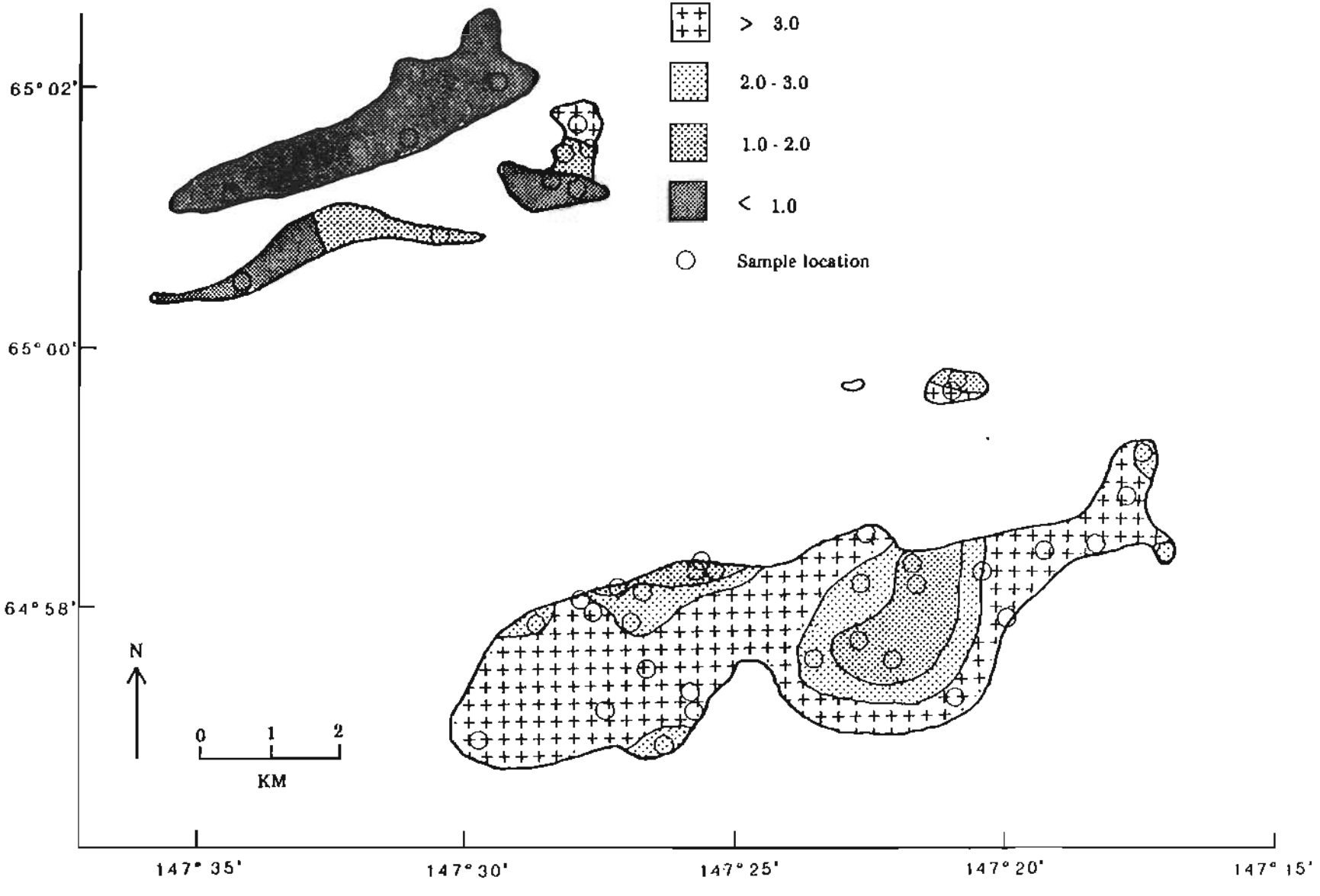

Figure 12. Distribution of the $K_2O + Na_2O$ to $FeO_{total} + MgO$ ratio, Gilmore Dome and Pedro Dome samples.

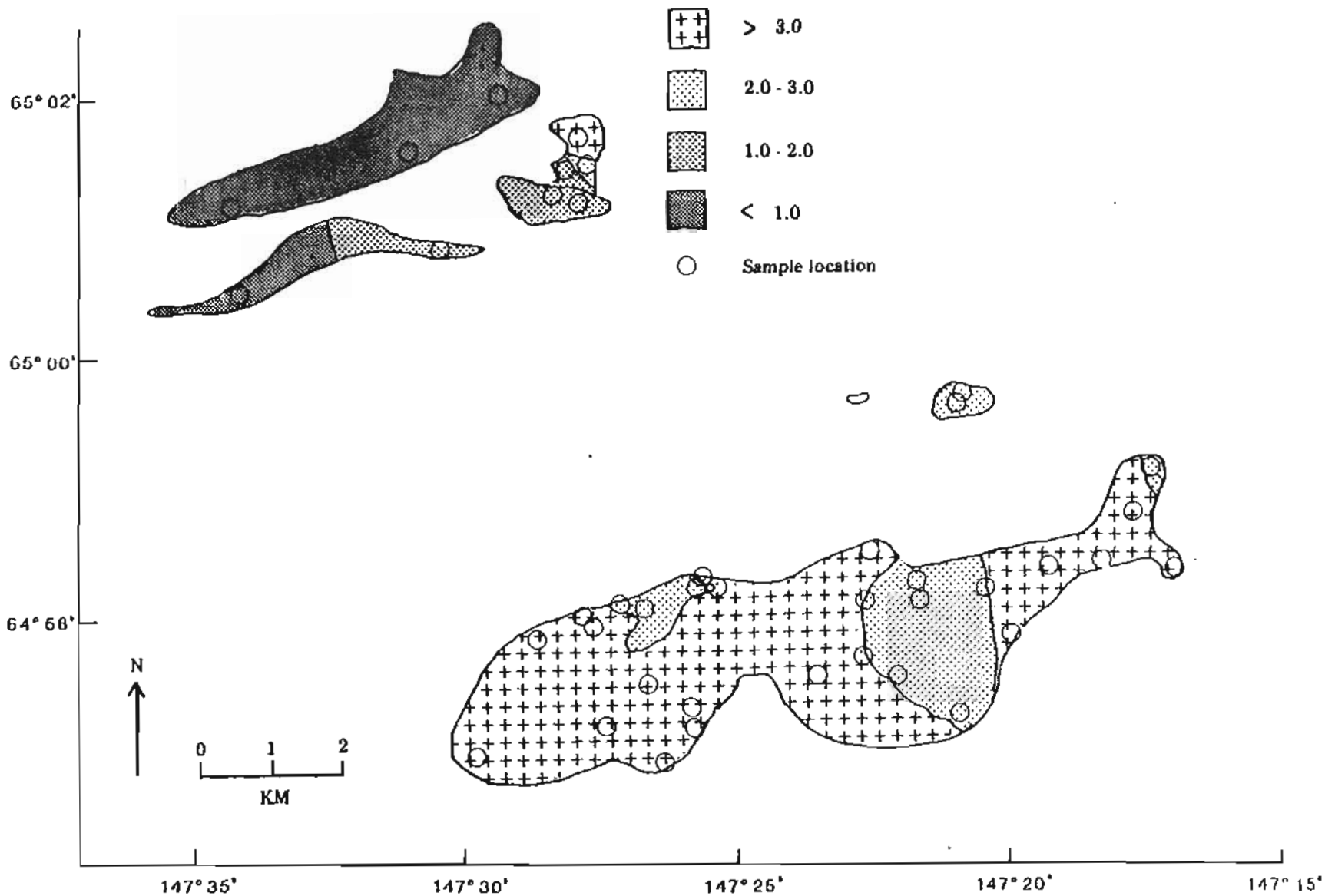

Figure 13. Distribution of the $Na_2O + K_2O$ to CaO ratio, Gilmore Dome and Pedro Dome samples.

PRESSURE AND TEMPERATURE OF INTRUSION

Experimental investigations by Tuttle and Bowen (1958) in the system $NaAlSi_3O_8$-$KAlSi_3O_8$-SiO_2-H_2O illustrate the shift in the minimum melting composition of the synthetic granite system with increased pressure. The residual melt compositions of plutonic rocks have been compared with the minimum melting compositions in the synthetic granite system at various water pressures in order to estimate temperature and pressure conditions during intrusion of plutonic rocks (Putman and Alfors, 1965; Swanson, 1978).

Natural granite systems are more complex than Tuttle and Bowen's (1958) synthetic granite system, which limits the application of pressure-temperature estimates based on the synthetic system. Granitic rocks usually contain additional components such as calcium, iron, and magnesium. In addition, the experiments of Tuttle and Bowen (1958) were performed in the presence of a water-rich vapor phase that is a condition not commonly encountered during 'natural' crystallization. Therefore, analyses of aplite dikes from the Gilmore Dome pluton were used for comparison with the synthetic system because they represent the late-stage residual liquid. They are composed primarily of components of the synthetic system, and the presence of aplite-pegmatite dikes has been interpreted as evidence for vapor saturation during emplacement (Jahns and Tuttle, 1963). Analyses of the five aplite dikes are given in appendix F. Normative Ab+Or+Qtz ranges from 91 to 94 percent, while normative anorthite ranges from 0.7 to 4.7 percent.

Although the aplite dikes closely approximate the synthetic system, additional components are present and may cause melting relationships within the natural system to differ from those of the synthetic system. James and Hamilton (1969) show that the addition of small amounts of $CaAl_2Si_2O_8$ to the $NaAlSi_3O_8$-SiO_2-H_2O system causes an apparent shift in the minimum melting composition. Because of the nature of this shift, pressure estimates based on compositions in the synthetic granite system are minimums when $CaAlSi_2O_8$ is present (Jahns and Hamilton, 1969). It is also possible that CO_2 and F_2 could have been present in addition to water in the vapor phase. The presence of volatiles other than water may change phase relations in granitic systems (Wyllie and Tuttle, 1961) and cause a shift in the quaternary minimum defined by Tuttle and Bowen (1958). Any of these deviations from the synthetic system could cause inaccuracies in the pressure-temperature estimates that would cause pressure estimates to be minimum values and temperature estimates to be maximum values (Swanson, 1978).

However, the results do show excellent agreement with the experimental curve (fig. 14) and are considered a reasonable approximation. Putman and Alfors (1965) and Swanson (1978) consider their pressure-temperature estimates using the simplified system to be valid approximations based on similar data. The compositions of the aplite dikes fall very near the trend of the isobaric minima as water pressure is varied. The average of five dike compositions corresponds to water pressure = 1.2 kbar, and the range of compositions corresponds to water pressure from about 0.9 to 1.5 kbars.

An estimate for the depth of intrusion of the Gilmore-Pedro plutons can be made if we assume water pressure = lithostatic pressure. This assumption

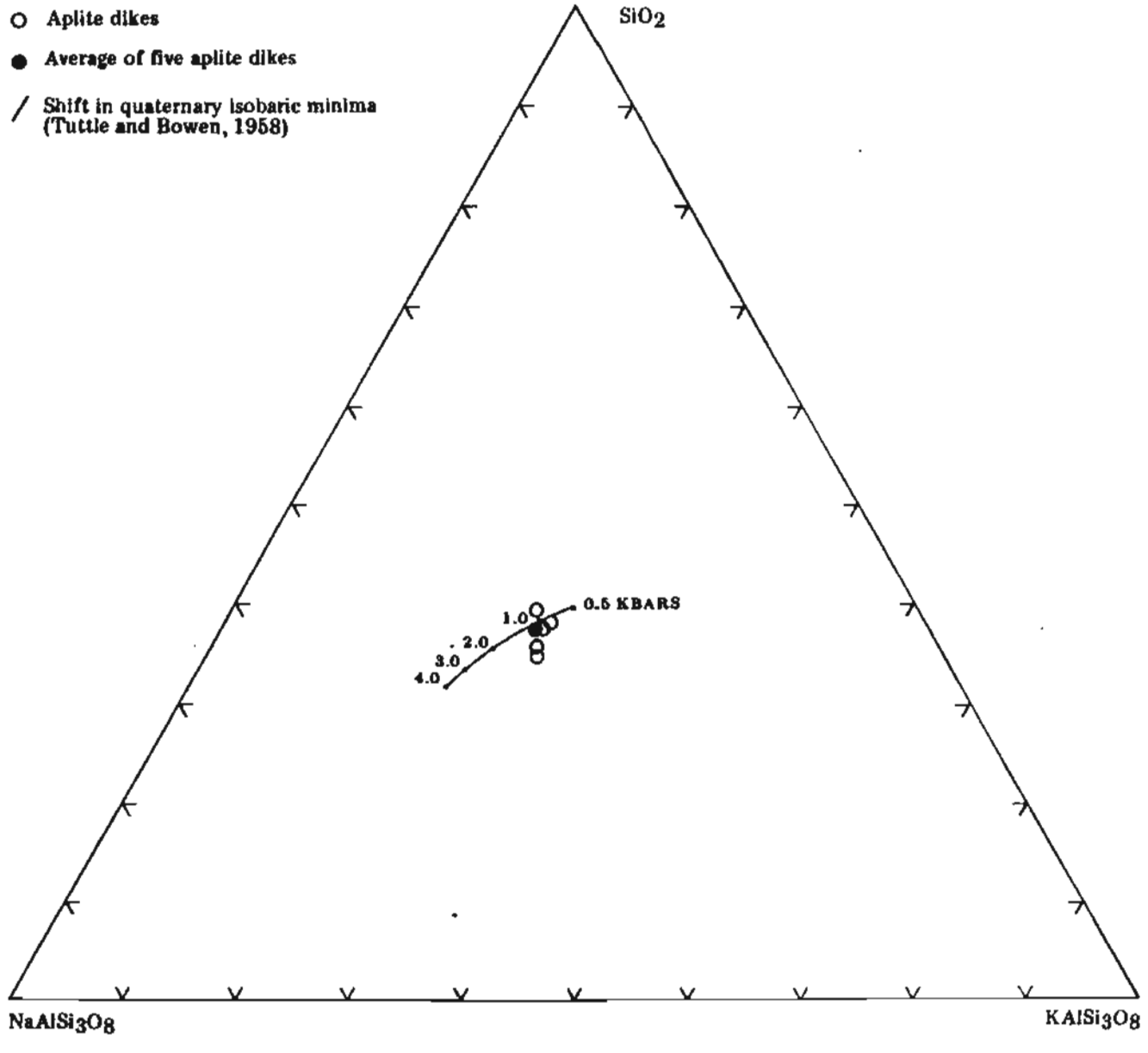

Figure 14. Plot of normative albite, orthoclase, and quartz for the analyzed dikes and the synthetic granite system.

can be made because the forceful injection of the aplites is interpreted to have occurred when water pressure reached and then slightly exceeded lithostatic pressure (Jahns and Tuttle, 1963). If we assume the density of schist in the Fairbanks district is nearly equal to the average density for schists (1.64 gm/cm^3)(Telford and others, 1976), then the pressure gradient caused by the weight of overlying rocks is 0.259 kbars/km. This corresponds to a minimum emplacement depth of 3.5 to 5.8 km.

The temperature of crystallization of the residual aplitic magma can also be estimated from the experimental results of Tuttle and Bowen's (1958) synthetic granite system. At water pressure = 1.2 kbar, the minimum liquidus temperature corresponds to about 720°C. The range of minimum temperatures corresponding to the range in water pressure is about 705° to 740°C.

RUBIDIUM AND STRONTIUM ISOTOPES

Introduction

To determine the isotopic composition of rubidium and strontium in each intrusive phase, whole-rock samples were analyzed by Teledyne Isotopes of Westwood, New Jersey. Six samples were chosen based on two criteria: a) freshness of the sample, and b) maximum spread of rubidium-strontium ratios between the samples.

The radioactive isotope ^{87}Rb decays to stable ^{87}Sr by beta-particle emission with a half life of 48.8×10^9 yr (Steiger and Jager, 1977). Therefore, the parent-daughter relationship between ^{87}Rb and ^{87}Sr can be used to determine the age and initial isotope composition of a suite of comagmatic rocks. The decay constant corresponding to a half life of 48.8×10^9 yr is 1.42×10^{-11}. The age formula derived from the standard exponential decay equation is:

$$age = 1.42 \times 10^{11} \ln(1 + {}^{87}Sr/{}^{87}Rb).$$

The absolute number of ^{87}Sr and ^{87}Rb atoms is difficult to determine in the laboratory. The more easily and more accurately determined ratios of ^{87}Sr and ^{87}Rb to the stable isotope ^{86}Sr are reported instead, because the total number of ^{86}Sr atoms in a sample remains constant through time.

The values of $^{87}Sr/^{86}Sr$ and $^{87}Rb/^{86}Sr$ for the Gilmore-Pedro intrusive suite are given in appendix H and plotted on an isochron diagram in figure 15. During fractional crystallization, the amount of rubidium in the suite of rocks increases causing the $^{87}Rb/^{86}Sr$ ratio to increase. It can be seen in figure 15 that the $^{87}Rb/^{86}Sr$ ratio increases from the fine-grained granodiorite to the porphyritic granodiorite to the porphyritic quartz monzonite to the aplite dikes. The $^{87}Sr/^{86}Sr$ ratio does not change with fractional crystallization, so that at the time of crystallization all intrusive phases had the same initial $^{87}Sr/^{86}Sr$ ratio. The observed variation in $^{87}Sr/^{86}Sr$ is a result of radioactive decay of ^{87}Rb to ^{87}Sr since the time of fractionation of the magma. More evolved phases incorporated greater amounts of ^{87}Rb and have therefore produced more radiogenic ^{87}Sr.

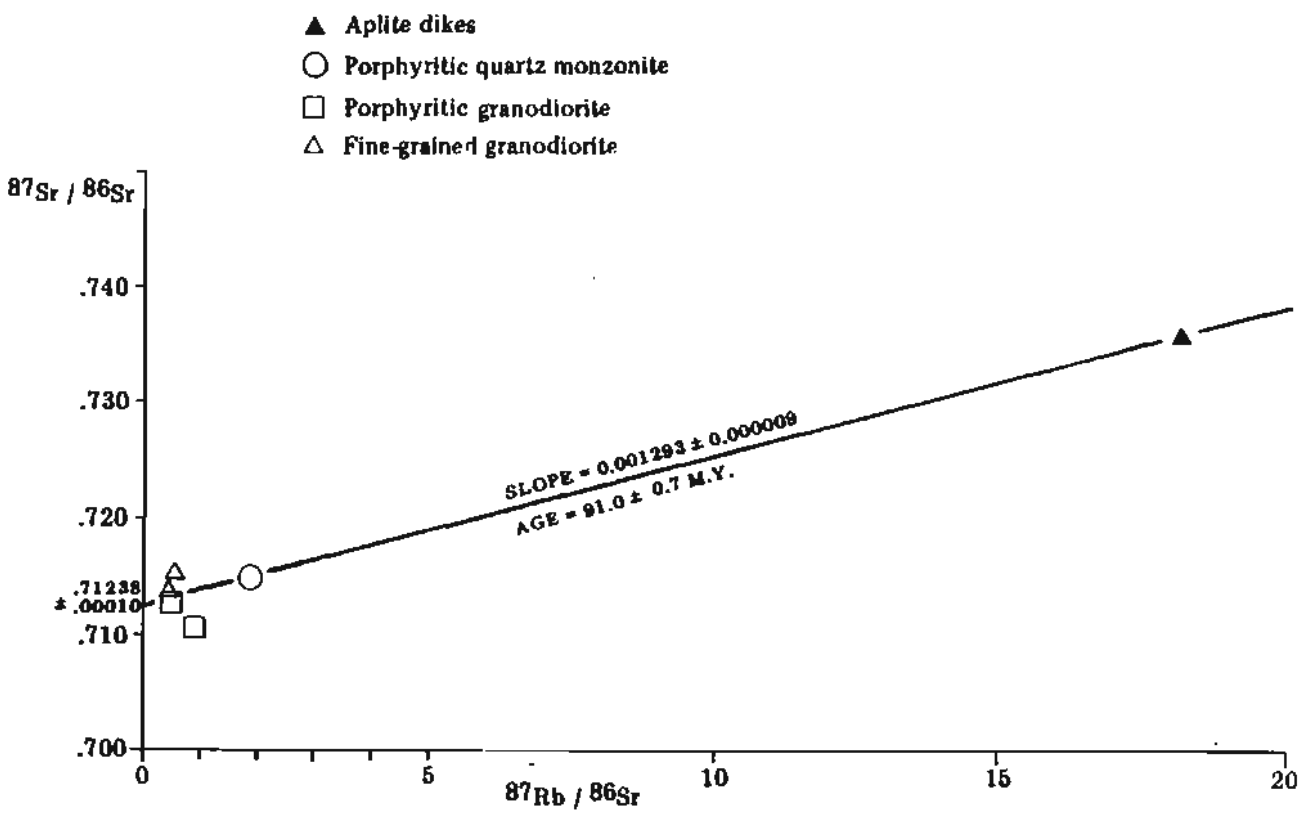

Figure 15. Values of $^{87}Sr/^{86}Sr$ and $^{87}Rb/^{86}Sr$ for the Gilmore Dome and Pedro Dome intrusive suite plotted on an isochron diagram.

All members of a comagmatic suite of rocks that have the same age, the same initial $^{87}Sr/^{86}Sr$ ratio, and remain closed to rubidium and strontium will form a straight line on the isochron diagram. The slope of the line equals the $^{87}Sr/^{87}Rb$ ratio and is used to determine the age of crystallization, while the intercept of the line is equal to the initial $^{87}Sr/^{86}Sr$ ratio at the time the system became closed. The isochron would have a slope of zero at the time of crystallization before any radioactive decay began, and with time the line would pivot about the initial $^{87}Sr/^{86}Sr$ value steadily increasing in slope. Each point on the isochron moves as a function of time along a straight line with a slope of -1 because each decay reduces the number of ^{87}Rb atoms by one and increases the number of ^{87}Sr atoms by one.

Gilmore-Pedro Isochron

A total of six samples were analyzed for rubidium and strontium isotopes from the Gilmore-Pedro intrusive suite. Three samples from the relatively large and compositionally variable Gilmore Dome pluton were collected in an attempt to establish a good isochron. Analyzed rubidium-strontium ratios varied from 0.228 to 10.29. Three samples with the greatest range in values were chosen, which corresponded to one sample from each intrusive phase.

At Pedro Dome the rubidium-strontium ratios of the fine-grained granodiorite had only a small variation---from 0.152 to 0.229---too small to establish a good isochron. The two most variable samples were used to test whether the fine-grained granodiorite plotted along the Gilmore Dome isochron. Finally, a sample of porphyritic granodiorite from the small pluton on Pedro Dome was included to test whether it plotted on the Gilmore Dome isochron. Figure 15 is an isochron diagram that gives results of the isotope analyses. The isochron line was fit to the data points using the statistical regression method of York (1969), as suggested by Brooks and others (1972).

Due to the highly fractionated nature of the aplite-dike sample, its $^{87}Rb/^{86}Sr$ ratio is nearly one order of magnitude greater than the other samples. For this reason, the slope of the isochron depends very heavily on the position of the aplite-dike data point. Chemical alteration of the sample or country-rock assimilation by the aplite dike could alter the rubidium-strontium systematics and change the position of the data point on the isochron diagram. This could greatly alter the slope of the isochron and thus the estimated age. Thin-section analysis of the aplite dike (sample 138b) indicates no observable chemical alteration; it is one of the freshest samples collected from the plutons. The intrusion of the aplite dike into the porphyritic quartz monzonite pluton makes country-rock assimilation unlikely. The reliability of the aplite-dike data point is therefore not in question, and a great deal of confidence is placed on the slope of the calculated isochron.

It is obvious that two data points from Pedro Dome do not fall on the isochron. The deviation is greater in magnitude than the reported experimental error and is therefore termed geological error (McIntyre and others, 1966). For this reason, the isochron computer program of Teledyne Isotopes removed these points in calculation of the 'best isochron.' This isochron, based on the four data points, corresponds to an age of 91.0 ± 0.7

m.y. and an initial $^{87}Sr/^{86}Sr$ ratio of 0.71238 ± 0.00010. For comparison only, all six points were used to fit a straight line. This line is termed an errorchron (Brooks and others, 1972). The age corresponding to the errorchron is 90.4 m.y. with an initial $^{87}Sr/^{86}Sr$ ratio of 0.71244. Finally, an isochron was calculated for the three Gilmore Dome pluton samples exclusively; the age was calculated as 90.0 m.y. with an initial $^{87}Sr/^{86}Sr$ ratio of 0.71238.

The two sample points that do not fit the isochron are attributed to 'geologic error' (McIntyre and others, 1966), which includes all sources of error that occur outside the laboratory. The geometry of the data points, along with geological arguments, preclude the possibility that the anomalous points define a second isochron. The anomalous points can be explained only if the rocks have not been a closed system with respect to rubidium and strontium during their history. Sample 215 lies below the isochron, which indicates that it has either been enriched in rubidium relative to strontium or has lost ^{87}Sr relative to ^{86}Sr. Sample 211 lies above the isochron, which indicates a decrease in the rubidium-strontium ratio or an increase in the $^{87}Sr/^{86}Sr$ ratio.

Dasch (1969) and Bottino and Fullagar (1968) found that progressive chemical weathering and alteration of granitic rocks caused an increase in rubidium-strontium ratios of up to 70 percent, while the $^{87}Sr/^{86}Sr$ ratio remained constant or increased slightly. Chemical weathering and alteration probably explain the anomalous position---to the right of the isochron---of sample 215, which is from the very small porphyritic granodiorite pluton near Pedro Dome. The pluton is located near and dissected by several hydrothermal shear zones. In thin section, nearly one-third of the mafics are altered to chlorite and epidote. The rock also has a great deal of secondary carbonate that has probably altered the abundance of strontium with the introduction of secondary calcium. The alteration is far more extensive in this sample than in any others selected for rubidium- and strontium-isotope analysis. This alteration probably caused the geologic error by increasing the rubidium-strontium ratio and causing the data point to plot below the isochron.

Faure and Powell (1972) discuss various mechanisms by which magmas may become contaminated with foreign strontium from the wall rocks, resulting in a variation in the $^{87}Sr/^{86}Sr$ and $^{87}Rb/^{86}Sr$ ratios. Al-Rawi and Carmichael (1967) propose that radiogenic strontium in rubidium sites in mica and potassium feldspar would be more mobile than nonradiogenic strontium and would move more rapidly into adjacent magma. Pankhurst (1969) suggests that anomalously high $^{87}Sr/^{86}Sr$ ratios might be produced by isotopic exchange or equilibrium between a hydrous magma and the country rock. Finally, bulk assimilation of wall rock high in radiogenic strontium would produce higher $^{87}Sr/^{86}Sr$ ratios in the magma, especially near contacts. Any combination of these mechanisms could cause the geologic error by increasing the $^{87}Sr/^{86}Sr$ ratio in sample 211, which would allow the data point for sample 211 to plot above the isochron. Sample 211 is a rubble sample collected from the narrow tip of an elongate pluton on Pedro Dome. Because the pluton is approximately 0.30 km wide at that point, the sample came from within 0.15 km of the nearest wall-rock contact. Whole-rock chemistry indicates that sample

211 has the highest SiO_2 and K_2O content of all fine-grained granodiorite samples and the lowest content of CaO, MgO and $FeO_{(total)}$. The proximity to a contact, along with the relatively felsic chemistry, make some type of wall-rock contamination a probable cause for the anomalously high $^{87}Sr/^{86}Sr$ ratio in sample 211.

AGE AND ORIGIN OF MAGMA

Radiogenic Isotopes

As discussed in a previous section, the 'best estimate' of the isochron slope is 0.001293 ± 0.000009, which yields an age of 91.0 ± 0.7 m.y. and an initial $^{87}Sr/^{86}Sr$ ratio of 0.71238 ± 0.00010. These values were reported by Teledyne Isotopes using an isochron computer program based on the line fitting method of York (1969).

The age estimate from the Gilmore isochron is 90.9 m.y.; the errorchron, using all data points, gives an age estimate of 90.4 m.y. All values are within the error bars of the 'best isochron' age of 91.0± 0.7 m.y., and therefore this age is accepted as valid.

Potassium-argon radiometric dating has been performed on two samples from the Gilmore-Pedro suite. Hornblende from the fine-grained granodiorite near sample locality 205 yielded an age of 90.7 ± 5.1 m.y. (Britton, 1970). Biotite from the porphyritic quartz monzonite near sample locality 215 yielded an age of 93.0 ± 5.0 m.y. (unpublished data cited by Britton, 1970). The potassium-argon and rubidium-strontium ages are in complete agreement within analytical error. This indicates that since the time of crystallization about 91 m.y. ago, there have been no thermal metamorphic events with sufficient heat to reset the potassium-argon age, which means that the temperature did not exceed the biotite blocking temperature for argon (approximately 230°C) (Damon, 1968).

The initial $^{87}Sr/^{86}Sr$ ratio of about 0.7124 for the isochron places constraints on models for the origin of magma. Figure 16 illustrates the usual range of initial $^{87}Sr/^{86}Sr$ ratios for various types of rocks. The initial ratio of 0.7124 is much higher than other major Phanerozoic batholiths that are derived primarily from mantle or lower crustal sources (Kistler, 1974; Armstrong and others, 1977).

The relatively high initial ratio rules out primary mantle or lower crustal sources for the Gilmore-Pedro magma. The initial ratio of 0.7124 suggests the magma is primarily derived from Precambrian crustal source rocks. It could either be derived entirely from Precambrian metamorphic rocks with an initial $^{87}Sr/^{86}Sr$ ratio of about 0.7124, or it could be derived from a mantle or lower crustal magma similar to the major Phanerozoic batholiths (fig. 16) that assimilated large volumes of Precambrian metamorphic rocks during emplacement. A combination of the above mechanisms is also a possible source for the magma.

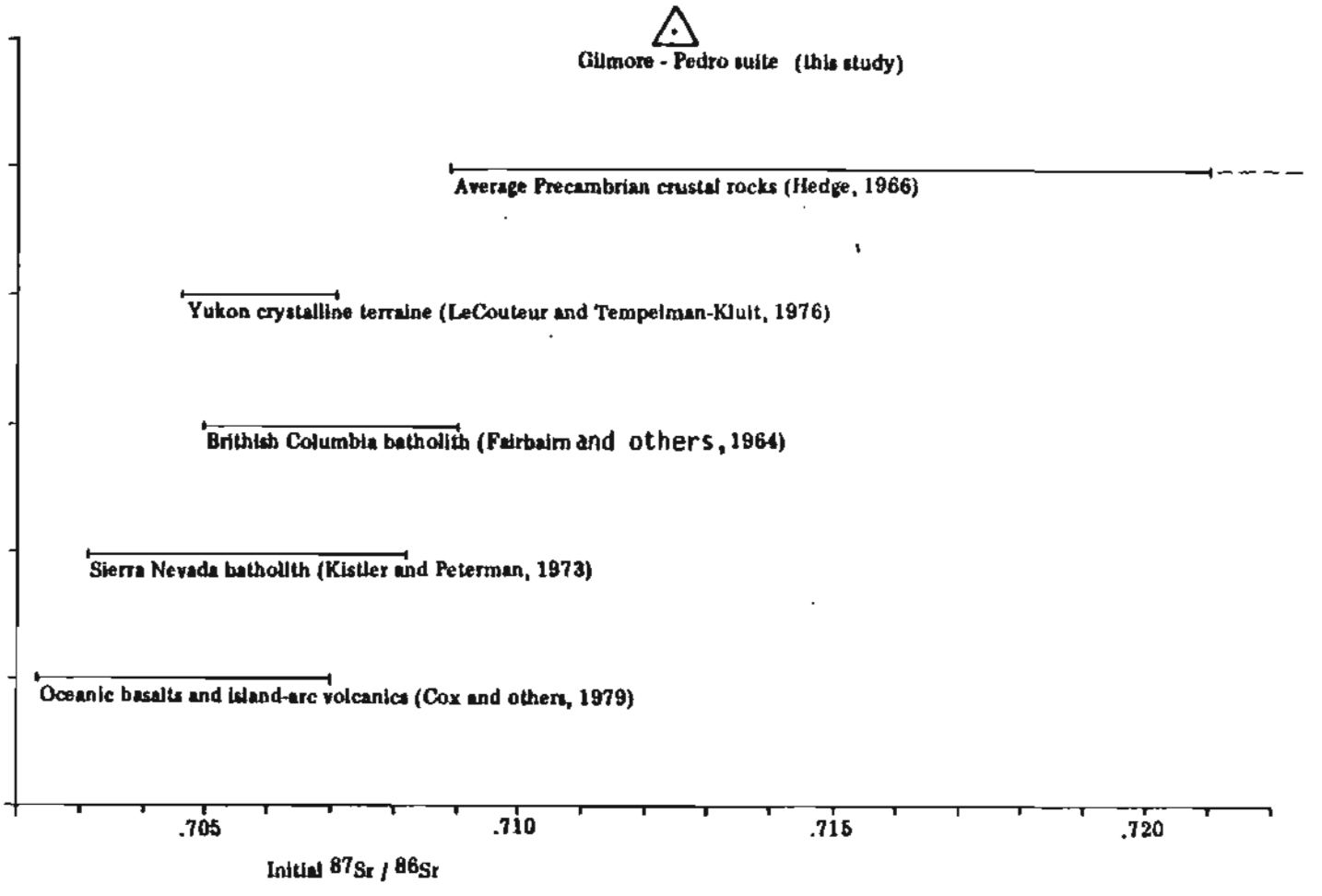

Figure 16. Comparison of initial $^{87}Sr/^{86}Sr$ in the Gilmore Dome and Pedro Dome suite with other rock types and major batholiths.

Metamorphism of Country Rocks

The minimum temperature necessary for the first stages of granitic melting is about 630°C, and even higher temperatures---in excess of 700°C---are necessary at the low water pressures of 0.9 to 1.5 kbar under which the Gilmore-Pedro plutons crystallized (Winkler, 1979). Metamorphic mineral assemblages in both mafic and pelitic rocks in the Fairbanks mining district are low grade and indicate that metamorphic temperatures were probably below 510°C (Winkler, 1979). The characteristic mafic mineral assemblage is:

> actinolitic-hornblende + albite-oligoclase + epidote
> (Brown, 1962).

The characteristic pelitic mineral assemblage is:

> quartz + albite + muscovite + chlorite + biotite + garnet
> (Brown, 1962).

One whole-rock analysis is available for a mafic metamorphic rock (Forbes, 1982). For this composition and mineral assemblage, the metamorphism is considered low grade (Winkler, 1979). Whole-rock chemical analyses are not available for the pelitic rocks. However, the stable assemblage garnet + chlorite + muscovite is definitive, and places the pelitic schist in Winkler's low-grade zone (Winkler, 1979).

Figure 17 (modified from Winkler, 1979) shows metamorphic grades plotted on a pressure-temperature grid. Boundaries between the fields represent experimentally determined metamorphic reactions for pelitic and mafic compositions. The stable pelitic assemblage (biotite + muscovite) and the stable mafic assemblage (hornblende + albite) in the Fairbanks schists indicate that temperatures were to the right of the very low grade field. The stable pelitic assemblage (garnet + chlorite) and the low An content of the plagioclase in the mafic rocks constrains the metamorphic temperatures to the left of the medium-grade field (Winkler, 1979). The low-grade field is the pressure-temperature region that describes the metamorphism of the country rock in the Pedro and Gilmore Dome areas. Metamorphic temperatures were between about 475°C and 510°C. Also plotted on figure 17 is the minimum anatectic melting curve. It is obvious that the low-grade metamorphism at the present level of exposure in the Fairbanks district was too cool for anatectic melting.

Thermal History

As discussed previously, potassium-argon and rubidium-strontium ages for intrusive rocks in the Gilmore and Pedro Dome areas cluster closely around 91 m.y. Potassium-argon mica ages for six metamorphic rock samples in the Fairbanks mining district range from 100 ± 3.0 m.y. to 131.0 ± 2.0 m.y. and average about 122 m.y. One metamorphic amphibole potassium-argon analysis gave an age of 240 ± 18 m.y. (Forbes, 1982). Forbes (1982) attributes the potassium-argon age discordance to the higher blocking temperature of amphibole compared to mica.

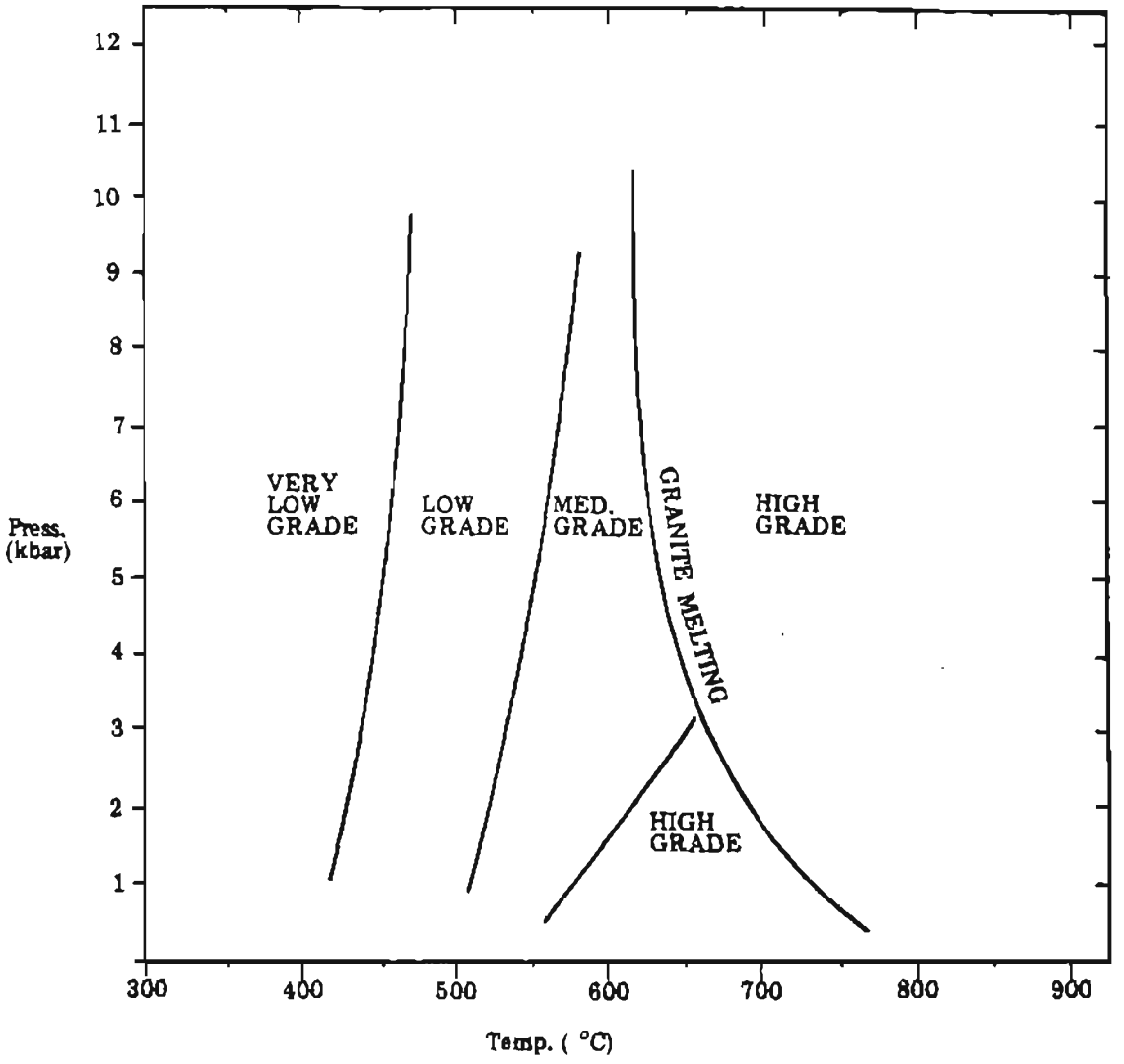

Figure 17. Grades of metamorphism (modified from Winkler, 1979).

Given the above interpretation of the radiometric dates and the metamorphic temperature constraints based on stable mineral assemblages, the following thermal history for the Fairbanks schists is implied. Prior to 240 m.y. ago, metamorphic temperatures of the Fairbanks schists peaked. At about 240 m.y. ago, the schists cooled through the amphibole blocking temperature of about 475°C (Damon, 1968) for the last time. Between about 100 and 131 m.y. ago, metamorphic temperatures cooled through the mica blocking temperature of about 230°C (Damon, 1968) for the last time. Therefore, at about 91 m.y. ago, when the plutons were intruded, metamorphic temperatures of the country rock were below 230°C, which is far below minimum temperatures of anatectic melting.

The rocks that anatectically melted to form the intrusives in the Fairbanks mining district were metamorphosed at a higher grade than the maximum grade of metamorphism that was probably attained by the rocks

currently exposed in the Fairbanks mining district. This indicates that source rocks for the magma were at far greater depths than the rocks currently exposed in the Fairbanks mining district.

Implications for Tungsten-Ore Genesis

Igneous rocks are most frequently assumed to be the source of lode-metal deposits (Krauskopf, 1967). The best evidence for a genetic relationship between the intrusive rocks and mineralization in the Fairbanks mining district, as well as on a world-wide scale, is geographic association. The tendency of ore deposits to cluster near the borders of granitic intrusives is obvious and has long been used as a successful prospecting tool (Krauskopf, 1967).

There are over 10 tungsten and tungsten-gold prospects along the northern contact of the Gilmore Dome stock. Several tungsten occurrences have been mined, and one deposit on Gilmore Dome is currently mined. The occurrences near Gilmore Dome are located near the contact with the Gilmore Dome pluton. The intrusion of the pluton during Cretaceous time altered the country rock and produced calcite-epidote skarns and calcite-diopside skarns that host the tungsten mineralization locally (Robinson and Metz, 1979).

Maucher (1976) suggests that tungsten deposits associated with granites derived their tungsten from older strata-bound scheelite deposits during crustal melting. Many strata-bound tungsten deposits and occurrences are now considered to be submarine volcanic exhalative in origin (Holl, 1977; Stumpf, 1977). According to Plimer (1980), strata-bound tungsten deposits invariably occur in Proterozoic to early Paleozoic sequences of thick pelitic metasediments associated with mafic volcanic rocks and carbonates. Metz (1977) compared the strata-bound tungsten occurrence of the Circum-Pacific described by Maucher (1976) with the mercury-antimony-tungsten occurrences in Alaska and suggested a strata-bound model for many of the Alaskan occurrences. Some units of the Fairbanks mining district schists may contain strata-bound tungsten accumulations (Metz and Robinson, 1980).

Foster (1977) has shown experimentally and in field relations that scheelite can be remobilized during low-grade greenschist metamorphism. Plimer (1980) suggests that during anatexis of metasediments, elements such as tungsten, molybdenum, tin, fluorine, and bismuth are mobile and would be the first components to partition readily from calc-silicate rocks into the melt. The first components to partition into the anatectic melt are those that are not readily accommodated in silicate structures, and therefore tungsten occurrences are associated with late-stage, highly fractionated, leucocratic, generally potassic granites. Anatexis of sequences containing exhalative tungsten deposits could provide a mechanism for reconcentration. Reconcentration into the residual melt fractions and late-stage aqueous fluids could concentrate tungsten from an exhalative deposit into a deposit associated with granites.

Groves and McCarthy (1978) stress the importance of modeling fractional crystallization histories for metal-bearing granitoids as a mineral- exploration technique. They discuss the use of rubidium- and strontium-isotope

studies, major-element geochemistry, and trace-element geochemistry in the development of crystallization models. A crystallization model based on systematic changes in geochemistry provides a useful tool for assessing the metal potential of a granitoid and for indicating the mechanisms of crystallization of the magma, and hence the source and location of possible ore (Groves and McCarthy, 1978).

There are several possible models for the formation of the tungsten mineralization associated with the Gilmore Dome intrusive stock. One model calls for anatectic melting of volcanic-exhalative strata-bound tungsten deposits in the country rock, and subsequent concentration of tungsten in the late-stage melt during crystallization of the Gilmore Dome stock. Another model calls for a primary, upper-mantle or lower-crustal source for the granite and associated tungsten mineralization. Partial melting of the upper mantle or lower crust could produce an intrusive stock of the appropriate composition and could also be the source of the associated metals. A final model suggests that the metals are generated by a process that has nothing to do with the intrusive stock. Rather they are concentrated near intrusive contacts, either because the stocks provided convenient channel ways for the ore-bearing fluids, or because the stocks merely provided the heat or fluids necessary to remobilize metals in the country rock.

The findings of this study place constraints on possible models of tungsten-ore genesis. The high initial $^{87}Sr/^{86}Sr$ ratio of 0.7124 rules out the possibility that the intrusives and associated mineralization are of primary mantle origin. They must instead be derived from remelted Precambrian crustal rocks.

The model that calls for the anatectic melting of strata-bound tungsten accumulations in the Fairbanks schist and reconcentration during fractional crystallization can also be ruled out. The problem with this model is that it requires anatectic melting of low-grade metamorphic rocks that were far below anatectic temperatures at the time of granitic emplacement.

Given the petrologic constraints discussed in this thesis, only a few possible models remain for the origin of the tungsten mineralization at Gilmore Dome. One possibility is the model in which the metals were wholly derived from the Fairbanks mining district schists and were concentrated near intrusive contacts because the contacts provided convenient channelways for ore-bearing fluids, or because the plutons provided the heat or fluids necessary to remobilize disseminated metals in the country rock. The second possibility is that the metals were derived from high-grade metamorphic rocks that were at a far greater depth than the rocks currently exposed. The anatectic melting of a metal-rich metamorphic assemblage could have caused the metals to concentrate in the granitic magma. Intrusion of the magma may have altered the country rock and produced skarns that host the mineralization locally.

SUMMARY OF INTRUSIVE HISTORY

Anatexis of Precambrian, high-grade metamorphic rocks produced a granitic magma deep within the earth's crust about 91 m.y. B.P.. The magma rose to

shallower depths within the crust where a combination of lower temperatures and pressures caused the magma to crystallize. Fractional crystallization of this magma produced the compositional variation that exists between the four different phases of the Gilmore-Pedro fractionation suite. As the parental magma chamber crystallized inward, high-temperature minerals such as plagioclase and mafics crystallized first, causing the remaining magma to become progressively more felsic in composition.

Throughout crystallization, apophyses of magma left the chamber and intruded higher (about 4-km depth) into the crust to the present level of exposure, and passively filled the cores of large structural antiforms. The fine-grained granodiorite plutons intruded first and crystallized. These represent the least differentiated magma that most closely resembles the initial composition of the parental magma. A second pulse of magmatic emplacement is represented by the more felsic porphyritic granodiorite plutons. One of these plutons intruded the already solidified contact zone of the smallest fine-grained granodiorite pluton at Pedro Dome. The final pulse of magmatic emplacement from the parental magma chamber is represented by the very felsic porphyritic quartz monzonite plutons. The porphyritic quartz monzonite intruded beside the porphyritic granodiorite pluton at Pedro Dome and surrounded the porphyritic granodiorite pluton at Gilmore Dome on three sides. Gradational contacts at both localities indicate that the porphyritic granodiorite was not yet solidified when the porphyritic quartz monzonite was emplaced.

As the porphyritic plutons crystallized, the magmas fractionated and became enriched in water. When water pressure exceeded lithostatic pressure, the residual magma fractured the already solidified boundary areas of the plutons and was intruded as aplite dikes and bodies.

REFERENCES CITED

Aleinikoff, J.N., Dusel-Bacon, Cynthia, Foster, H.L., and Futa, K., 1981, Proterozoic zircon from augen gneiss, Yukon-Tanana Upland, east-central Alaska: Geology, v. 9, p. 469-473.

Al-Rawi, Y., and Carmichael, I.S.E., 1967, Natural fusion of granites: American Mineralogist, v. 52, p. 1806-1814.

Armstrong, R.L., Tauberneck, W.H., and Hales, P.O., 1977, Rb-Sr and K-Ar geochronometry of Mesozoic granitic rocks and their Sr isotopic composition, Oregon, Washington, and Idaho: Geological Society of America Bulletin, v. 88, p. 397-411.

Bateman, P.C., 1961, Granitic formations in the east-central Sierra Nevada near Bishop, California: Geological Society of America Bulletin, v. 72, p. 1521-1538.

Bateman, P.C., and Chappell, B.W., 1979, Crystallization, fractionation, and solidification of the Tuolumne intrusive series, Yosemite National Park, California: Geological Society of America Bulletin, v. 90, p. 465-482.

Bottino, M.L., and Fullagar, P.D., 1968, The effects of weathering on whole-rock Rb-Sr ages in granitic rocks: American Journal of Science, v. 266, p. 661-670.

Britton, J.M., 1970, Petrology and petrography of the Pedro Dome plutons, Alaska: Fairbanks, University of Alaska M.S. thesis, 52 p.

Brooks, C., Hart, S.R., and Wendt, I., 1972, Realistic use of two-error regression treatments as applied to rubidium strontium data: Review of Geophysics and Space Physics, v. 10, p. 551-577.

Brown, J.M., 1962, Bedrock geology and ore deposits of the Pedro Dome area, Fairbanks mining district, Alaska: Fairbanks, University of Alaska M.S. thesis, 137 p.

Bundtzen, T.K., 1982, Bedrock geology of the Fairbanks mining district, western sector: Alaska Division of Geological and Geophysical Surveys Open-file Report 155, 2 sheets.

Byers, F.M. Jr., 1957, Tungsten deposits in the Fairbanks district, Alaska: U.S. Geological Survey Bulletin 1024-I, p. 199-216.

Cox, K.G., Bell, J.D., and Pankhurst, R.J., 1979, The interpretation of igneous rocks: London, George Allen and Unwin, Ltd., 450 p.

Damon, P.E., 1968, Potassium-argon dating of igneous and metamorphic rocks with application to the basin ranges of Arizona and Sonora, in Hamilton, E.I., and Farquhar, R.M., eds., Radiometric dating for geologists: London, Interscience Publishers, p. 1-72.

Dasch, E.J., 1969, Strontium isotopes in weathering profiles, deep-sea sediments, and sedimentary rocks: Geochemica et Cosmochimica Acta, v. 33, p. 1521-1552.

Fairbairn, H.W., Hurley, P.M., and Pinson, W.H., 1964, Initial Sr^{87}/Sr^{86} and possible sources of granitic rocks in southern British Columbia: Journal of Geophysical Research, v. 69, p. 4889-93.

Faure, G., and Powell, J.L., 1972, Strontium isotope geology: Berlin, Springer-Verlag, 188 p.

Forbes, R.B., 1982, Bedrock geology and petrology of the Fairbanks mining district, Alaska: Alaska Division of Geological and Geophysical Surveys Open-file Report 169, 68 p.

Forbes, R.B., and Brown, J.M., 1961, Preliminary geologic map of the Fairbanks mining district, Alaska: Alaska Division of Mines and Minerals Report 194-1.

Forbes, R.B., Pilkington, H.D., and Hawkins, D.B., 1968, Gold gradients and anomalies in the Pedro Dome-Cleary Summit area, Fairbanks district, Alaska: U.S. Geological Survey Open-file Report 68-101, 43 p.

Forbes, R.B., and Weber, F.R., 1982, Bedrock geologic map of the Fairbanks mining district, Alaska: Alaska Division of Geological and Geophysical Surveys Open-file Report 170, 2 sheets.

Foster, H.L., Weber, F.R., Forbes, R.B., and Brabb, E.E., 1973, Regional geology of Yukon-Tanana Upland, Alaska, in Arctic geology: American Association of Petroleom Geologists Memoir 19, p. 388-395.

Foster, R.P, 1977, Solubility of scheelite in hydrothermal chloride solutions: Chemical Geology, v. 20, p. 27-34.

Groves, D.I., and McCarthy, T.S., 1978, Fractional crystallization and the origin of tin deposits in granitoids: Mineralium Deposita, v. 13, p. 11-28.

Hedge, C.E., 1966, Variations in radiogenic strontium found in volcanic rocks: Journal of Geophysical Research, v. 71, p. 6119-26.

Holl, R., 1977, Early Paleozoic ore deposits of the Sb-W-Hg formation in the eastern Alps and their genetic interpretations, in Klemm, D.D., and Sneider, H.J., eds., Time and strata-bound ore deposits: Berlin, Springer-Verlag, p. 169-198.

Hutton, J.M., and Elliott, S.M., 1980, An accurate XRF method for the analysis of geochemical exploration samples and major and trace elements using one glass disc: Chemical Geology, v. 29, p. 1-11.

Jahns, R.H., and Tuttle, O.F., 1963, Layered pegmatite-aplite intrusives: Mineralogical Society of America Special Paper 1, p. 78-92.

James, R.S., and Hamilton, D.L., 1969, Phase relations in the system $NaAlSi_3O_8$-$KAlSi_3O_8$-$CaAl_2Si_2O_8$-SiO_2 at 1 kilobar water vapor pressure: Contributions to Mineralogy and Petrology, v. 21, p. 111-141.

Kistler, R.W., 1974, Phanerozoic batholiths in western North America: Annual Review of Earth and Planetary Sciences, v. 2. p. 403-418.

Kistler, R.W., and Peterman, Z.E., 1973, Variations in Sr, Rb, K, Na, and Initial Sr^{87}/Sr^{86} in Mesozoic granitic rocks and intruded wall rocks in central California: Geological Society of America Bulletin, v. 84, p. 3489-3512.

Krauskopf, K.B., 1967, Source rocks for metal-bearing fluids, in Barnes, H.L., ed., Geochemistry of hydrothermal ore deposits: New York, Holt, Rinehart, and Winston, Inc., p. 1-28.

Laniz, R.V., Stevens, R.E., and Norman, M.B., 1964, Staining of plagioclase feldspar and other minerals with F. D. and C. Red No. 2: U.S. Geological Survey Professional Paper 501-B, p. B152-B153.

LeCouteur, P.C., and Tempelman-Kluit, D.J., 1976, Rb/Sr ages and a profile of initial Sr^{87}/Sr^{86} ratios for the plutonic rocks across the Yukon crystalline terraine: Canadian Journal of Earth Sciences, v. 13, p. 319-330.

Maucher, A., 1976, The strata-bound cinnabar-stibnite-scheelite deposits, in Wolf, K.H., ed., Handbook of strata-bound and strataform ore deposits: Amsterdam, Elsevier, v. 10, p. 477-503.

McIntyre, G.A., Brooks, C., Compston, W., and Turek, A., 1966, The statistical assessment of Rb-Sr isochrons: Journal of Geophysical Research, v. 71, p. 5459-5468.

Mertie, J.B., Jr., 1937, The Yukon-Tanana region, Alaska: U:S. Geological Survey Bulletin 872, 276 p.

Metz, P.A., 1977, Comparison of mercury-antimony-tungsten mineralization of Alaska with strata-bound cinnabar-stibnite-scheelite deposits of the Circum-Pacific and Mediterranean region, in Short notes on Alaskan geology - 1977: Alaska Division of Geological and Geophysical Surveys Geological Report 55, p. 39-41.

_____, 1982, Bedrock geology of the Fairbanks mining district, northeast sector: Alaska Division of Geological and Geophysical Surveys Open-file Report 154, 1 sheet.

Metz, P.A., and Robinson, M.S., 1980, The investigation of mercury-antimony-tungsten metal provinces of Alaska II: Fairbanks, University of Alaska Mineral Industry Research Laboratory, unpublished.

Moore, J.G., 1963, Geology of the Mount Pinchot Quadrangle, southern Sierra Nevada, California: U.S. Geological Survey Bulletin 1130, 152 p.

Pankhurst, R.J., 1969, Strontium isotopic studies related to petrogenesis in the Caledonian basic igneous province of northeast Scotland: Journal of Petrology, v. 10, p. 115-143.

Plimer, I.R., 1980, Exhalative Sn and W deposits associated with mafic volcanism as precursors to Sn and W deposits associated with granites: Mineralium Deposita, v. 15, p. 275-289.

Prindle, L.M., Katz, F.J., and Smith, P.S., 1913, A geologic reconnaissance of the Fairbanks Quadrangle, Alaska: U.S. Geological Survey Bulletin 525, 220 p.

Putman, G.W., and Alfors, J.T., 1965, Depth of intrusion and age of the Rocky Hill stock, Tulare County, California: Geological Society of America Bulletin, v. 76, p. 357-364.

Robinson, M.S., 1982, Bedrock geology of the Fairbanks mining district, southeast sector: Alaska Division of Geological and Geophysical Surveys Open-file Report 146, 1 sheet.

Robinson, M.S., and Metz, P.A., 1979, Evaluation of the mineral resources of the pipeline corridor, phase I and II: Fairbanks, University of Alaska Mineral Industry Research Laboratory, unpublished.

Steiger, R.H., and Jager, E., 1977, Subcommission on geochronology: Convention on the use of decay constants in geo- and cosmo-chronology: Earth and Planetary Science Letters, v. 36, p. 356-362.

Stumpf, E.F., 1977, Sediments, ores, and metamorphism: New aspects: Philosophical Transactions of the Royal Society of London, v. 286, p. 507-525.

Swanson, S.E., 1977, Relation of nucleation and crystal-growth rate to the development of granitic textures: American Mineralogist, v. 62, p. 966-978.

_____, 1978, Petrology of the Rocklin pluton and associated rocks, western Sierra Nevada, California: Geological Society of America Bulletin, v. 89, p. 679-686.

Telford, W.M., Geldart, L.P., Sheriff, R.E., and Keys, D.A., 1976, Applied geophysics: Cambridge University Press, 860 p.

Thorne, R.L., Muir, N.M., Erickson, A.W., Thomas, B.I., Heide, H.E., and Wright, W.S., 1948, Tungsten deposits in Alaska: U.S. Bureau of Mines Report of Investigations 4174, 22 p.

Tuttle, O.F., and Bowen, N.L., 1958, Origin of granite in the light of experimental studies in the system $NaAlSi_3O_8$-$KAlSi_3O_8$-SiO_2-H_2O: Geological Society of America Memoir 74, 153 p.

Van Der Plas, L., and Tobi, A.L., 1965, A chart for judging the reliability of point counting results: American Journal of Science, v. 263, p. 87-90.

Wasserburg, G.J., Eberlein, G.D., and Lanphere, M.A., 1963, Age of Birch Creek schist and some batholithic intrusions in Alaska: Geological Society of America Special Paper 73, p. 258-259.

Winkler, H.G.F., 1979, Petrogenesis of metamorphic rocks: Berlin, Springer-Verlag, 348 p.

Wyllie, P.J., and Tuttle, O.F., 1961, Experimental investigations of silicate systems containing two volatile components (Pt. II); the effects of NH_3 and HF, in addition to H_2O, on the melting temperatures of albite and granite: American Journal of Science, v. 259, p. 128-143.

York, D., 1969, Least-squares fitting of a straight line with correlated errors: Earth and Planetary Science Letters, v. 5, p. 320,324.

APPENDIX A

Sample locations by latitude and longitude

sample number	latitude	longitude
101	64° 59.70'N	147° 23.00'W
106	59.65'	21.55'
108	59.75'	21.15'
116a	58.25'	20.55'
116b	58.20'	20.40'
117	58.25'	20.20'
119	58.35'	20.35'
124	58.35'	21.65'
127	58.30'	22.10'
128	58.15'	22.00'
129	58.05'	22.10'
130	57.85'	22.20'
131	58.50'	22.50'
132	58.15'	23.05'
133	58.20'	23.00'
134	57.60'	22.35'
135	57.70'	23.10'
137	58.65'	22.70'
138	58.35'	24.15'
139	58.30'	24.25'
141	57.95'	25.80'
142	58.25'	25.85'
143	58.15'	27.00'
144	58.15'	27.35'
145	57.95'	27.80'
146	58.25'	25.95'
147	58.35'	25.65'
148	57.90'	27.20'
149	57.55'	26.85'
150	57.45'	24.70'
152	57.35'	26.10'
155	57.65'	24.75'
157	57.90'	25.10'
160	58.05'	24.15'
161	57.60'	23.80'
162	58.10'	28.30'
165	57.20'	27.50'
166	57.20'	25.80'
167	56.85'	26.45'
170	56.90'	28.65'
173	57.25'	21.25'
175	57.85'	28.90'

sample number	latitude	longitude
177	64° 57.40'N	147° 29.25'W
178	57.60'	28.15'
179	56.80'	29.80'
180	58.85'	18.70'
182	58.50'	18.55'
183	58.50'	18.75'
185	58.75'	18.35'
186	58.35'	17.40'
187	58.70'	18.25'
189	58.35'	18.75'
190	58.25'	19.15'
191	58.00'	20.05'
194	58.40'	19.80'
195	59.10'	17.95'
201	65° 01.25'N	147° 34.50'W
202	01.55'	32.95'
203	01.60'	31.30'
204	02.15'	31.20'
205	02.10'	29.60'
207	00.55'	34.25'
208	00.90'	32.55'
209	01.15'	32.50'
211	00.85'	30.70'
212	02.00'	27.80'
213	01.55'	27.85'
214	01.70'	28.25'
215	01.55'	28.45'
216	01.35'	28.50'
217	01.25'	28.75'
218	01.25'	28.25'

APPENDIX B

Predicted standard deviation for a 400-point count

content in % by volume	% deviation at 95% confidence interval
5	2.2
10	3.0
15	3.5
20	4.0
25	4.2
30	4.4
35	4.6
40	4.8
45	4.9
50	5.0
55	4.9
60	4.8
65	4.6
70	4.4
75	4.2
80	4.0
85	3.5
90	3.0
95	2.2

APPENDIX C

Modal volume data for within-outcrop variation study

sample number	total points	percent by volume Kspar	Plag	Qrtz	Mafic
1	400	25	36	30	9
2	400	26	38	28	8
3	400	26	39	29	7
4	400	26	38	29	8
5	400	27	38	30	6
6	400	29	35	29	7
7	400	28	36	31	6
8	400	29	34	30	7

APPENDIX D

Modal volume for each rock type

Rock type: Porphyritic quartz monzonite

sample	slab point-count				thin-section estimate					
number	Kspar	Plag	Qrtz	Mafic	Biot	Horn	Chlo	Sphe	Epid	PrWm
116b	23	39	29	9	9	-	tr	tr	tr	-
117	33	35	23	9	8	-	1	tr	tr	-
124	27	38	34	1	1	-	tr	-	-	tr
131	32	32	28	8	3	3	1	tr	1	-
135	29	35	28	8	8	-	tr	tr	tr	tr
137	24	34	38	4	4	tr	tr	-	tr	tr
138a	30	30	36	4	4	-	tr	-	tr	tr
141	34	32	32	2	2	-	tr	-	-	tr
142	25	36	28	11	10	-	1	tr	-	tr
143	17	36	34	13	13	-	tr	tr	tr	tr
144	20	43	28	9	9	-	tr	tr	tr	tr
145	28	36	29	7	7	-	tr	-	-	tr
146	26	36	32	6	6	-	tr	tr	-	tr
148	27	36	26	11	11	-	tr	-	-	tr
149	34	36	26	4	4	tr	tr	tr	tr	tr
152	32	34	27	7	7	-	tr	-	tr	tr
155a	21	38	36	5	5	-	tr	-	-	tr
157	21	35	34	10	10	-	tr	-	tr	tr
160	18	38	34	10	no thin-section					
161	21	37	34	8	8	tr	tr	tr	tr	tr
165	25	39	30	6	6	tr	tr	tr	tr	tr
167	26	34	31	9	9	tr	tr	tr	tr	tr
170	31	38	22	9	9	tr	tr	tr	tr	tr
173	30	38	25	7	7	tr	tr	tr	tr	tr
175	28	31	33	8	8	-	tr	tr	-	tr
177	30	38	27	5	5	-	tr	-	-	tr
178	33	35	27	5	5	-	tr	-	-	tr
179	29	34	32	5	5	-	tr	-	-	tr
182	30	32	33	5	4	-	tr	tr	-	1
186	29	36	29	6	6	-	tr	tr	-	tr
187	23	35	32	10	9	-	1	tr	tr	tr
189	26	36	25	13	13	-	tr	tr	tr	tr
190	22	31	38	9	9	tr	tr	-	tr	-
192	26	37	29	8	8	-	tr	-	-	-
194	40	30	26	4	4	tr	tr	tr	tr	tr
195	19	41	30	10	10	tr	tr	tr	tr	tr
212	40	36	22	2	1	1	tr	tr	-	tr
214	35	36	26	3	3	tr	tr	tr	-	tr

Rock type: Porphyritic granodiorite

sample	slab point-count				thin-section estimate					
number	Kspr	Plag	Qrtz	Mafic	Biot	Horn	Chlo	Sphe	Epid	PrWm
101	28	46	17	9	no thin-section					
108	23	48	23	6	2	1	2	1	tr	-
116a	15	52	24	9	9	-	tr	tr	tr	tr
119a	13	52	30	5	4	tr	1	tr	tr	-
127	15	48	23	14	13	-	1	tr	tr	tr
128	11	51	29	9	9	-	tr	-	-	tr
129	14	46	32	8	7	-	1	tr	tr	tr
130	15	44	23	18	17	-	1	tr	tr	tr
132	19	54	21	6	5	-	1	tr	tr	tr
134	28	34	28	9	8	-	1	tr	tr	1
213	10	53	29	8	7	-	1	tr	tr	tr
215	14	53	19	14	7	4	2	1	tr	tr

Rock type: Fine-grained granodiorite

sample	slab point-count				thin-section estimate						
number	Kspr	Plag	Qrtz	Mafic	Biot	Horn	Cpyx	Opyx	Epid	Chlo	Sphe
201	10	45	19	26	10	10	-	-	1	5	-
202	10	47	22	21	10	8	-	-	tr	3	-
203	8	51	14	27	16	10	-	-	tr	1	tr
204	7	43	21	29	13	7	8	tr	tr	1	-
205	6	48	20	26	14	11	-	-	tr	1	tr
207	3	39	21	37	21	16	-	-	-	tr	-
208	2	41	21	36	16	20	tr	-	-	tr	-
209	6	43	25	26	15	11	-	-	tr	tr	-
211	8	46	29	17	9	6	-	-	tr	2	tr
216	9	45	25	21	11	10	-	-	tr	tr	tr
217	11	49	21	19	8	10	tr	-	tr	1	tr
218	9	47	23	21	11	9	tr	-	tr	1	tr

Rock type: Aplite dikes

sample number	slab point-count				thin-section estimate						
	Kspr	Plag	Qrtz	Mafic	Biot	Hema	Pyri	Garn	Chlo	Sphe	PrWm
119b	39	36	24	1	1	-	-	-	tr	tr	tr
133	36	30	31	1	-	-	1	-	-	-	2
138b	30	29	39	2	-	-	-	2	-	-	tr
139	38	34	27	1	1	-	-	tr	tr	-	tr
141	41	19	39	1	no thin section						
150	25	32	40	1	-	tr	1	-	-	-	2
155	35	33	32	0	tr	tr	-	-	tr	-	tr
166a	42	29	28	1	1	-	-	tr	tr	-	-
180	42	33	24	1	1	tr	-	-	tr	-	tr
183a	0	74	21	0	-	tr	-	-	tr	-	5
188	48	30	20	1	-	-	1	-	-	-	1
191	31	32	31	3	-	tr	tr	-	-	-	3

APPENDIX E

Rubidium-strontium data in ppm

sample number	Rb (ppm)	Sr(ppm)	Rb/Sr
106	140	690	0.203
127	105	460	0.228
138b	390	52	7.50
140	350	34	10.29
142	240	285	0.842
175	225	330	0.682
202	90	505	0.178
203	83	475	0.175
204	83	485	0.171
205	76	500	0.152
207	92	455	0.202
209	105	550	0.191
211	125	545	0.229
213	140	675	0.207
214	165	350	0.471
215	180	490	0.367

APPENDIX F

Whole-rock major-oxide data for each rock type in weight percent

Rock type: Porphyritic quaqtz monzonite

sample number	SiO_2	TiO_2	Al_2O_3	Fe_2O_3	FeO	MnO	MgO	CaO	Na_2O	K_2O	P_2O_5	total
135	74.95	0.28	11.85	0.47	2.84	0.10	0.47	1.98	2.76	3.40	0.10	99.20
137	77.67	0.07	12.13	0.20	1.13	0.04	0.00	1.37	3.37	3.68	0.04	99.70
142	71.15	0.28	14.50	0.45	2.93	0.08	0.54	2.36	3.28	3.66	0.08	99.31
143	70.00	0.29	14.23	0.27	2.57	0.08	0.51	2.33	3.24	3.59	0.09	97.20
144	69.65	0.41	13.58	0.46	3.33	0.10	0.95	2.22	2.79	4.01	0.14	97.64
145	74.72	0.14	14.38	0.29	1.53	0.06	0.24	1.66	3.14	4.46	0.09	100.71
146	71.76	0.32	12.75	0.41	2.79	0.10	0.56	2.13	2.90	3.47	0.09	97.28
148	71.43	0.25	13.90	0.42	2.61	0.17	0.42	2.21	3.21	3.41	0.07	98.10
149	74.85	0.07	13.05	0.11	1.32	0.04	0.00	1.48	3.39	3.90	0.07	98.28
152	74.30	0.12	12.52	0.18	1.55	0.06	0.03	1.58	3.25	3.95	0.06	97.60
161	72.95	0.20	14.40	0.64	1.49	0.07	0.38	1.91	3.03	4.46	0.07	99.60
162	76.68	0.05	12.89	0.35	0.54	0.10	0.11	0.96	3.69	4.56	0.12	100.05
165	72.88	0.19	13.79	0.41	0.19	0.07	0.30	1.95	3.28	4.13	0.08	97.27
166b	74.69	0.04	13.14	0.15	0.63	0.03	0.00	1.21	3.71	4.65	0.04	98.29
167	72.57	0.24	14.23	0.53	1.85	0.08	0.57	1.99	2.99	4.15	0.09	99.29
173	74.85	0.16	13.93	0.43	1.31	0.06	0.31	2.38	3.13	3.55	0.11	100.22
175	72.53	0.26	13.88	0.57	1.98	0.08	0.53	2.26	2.93	4.31	0.10	99.43
179	74.00	0.13	13.75	0.29	1.31	0.05	0.23	1.50	3.20	5.05	0.05	99.56
186	74.46	0.20	13.43	0.47	1.53	0.05	0.36	1.73	3.03	3.89	0.08	99.23
189	73.58	0.18	14.11	0.38	1.53	0.05	0.35	1.70	2.82	4.69	0.06	99.45
192	73.57	0.16	13.73	0.47	1.44	0.05	0.33	1.70	3.15	4.48	0.06	99.14
194	76.13	0.08	12.77	0.24	0.68	0.03	0.09	1.58	3.20	4.45	0.05	99.30
195	70.90	0.32	14.50	0.49	2.21	0.08	0.65	2.52	3.11	4.19	0.14	99.11
214	72.76	0.19	13.80	0.40	1.22	0.04	0.50	1.75	3.44	3.93	0.08	98.11

Rock type: Porphyritic granodiorite

sample number	SiO_2	TiO_2	Al_2O_3	Fe_2O_3	FeO	MnO	MgO	CaO	Na_2O	K_2O	P_2O_5	total
106	68.67	0.40	14.75	0.80	2.68	0.07	0.88	2.25	3.59	3.41	0.14	97.64
108	70.16	0.33	14.77	0.29	1.31	0.05	0.50	2.16	3.93	4.15	0.11	97.76
116a	72.52	0.29	13.98	0.47	1.49	0.04	0.52	2.34	3.24	4.05	0.08	99.02
127	69.76	0.49	14.80	0.58	2.61	0.06	0.96	2.85	3.17	3.13	0.12	98.53
128	70.30	0.47	14.83	0.68	2.12	0.05	0.80	2.72	3.04	3.66	0.15	98.82
132	71.61	0.37	14.76	0.40	1.94	0.04	0.67	2.37	3.39	3.71	0.13	99.39
134	74.08	0.26	13.02	0.57	2.52	0.09	0.45	2.06	2.87	3.37	0.10	99.39
213	70.61	0.40	14.80	0.65	2.16	0.05	0.66	2.97	3.53	3.09	0.15	99.07
215	67.03	0.57	15.05	0.95	3.15	0.09	1.07	3.53	3.54	3.00	0.19	98.17

Rock type: Fine-grained granodiorite

sample number	SiO_2	TiO_2	Al_2O_3	Fe_2O_3	FeO	MnO	MgO	CaO	Na_2O	K_2O	P_2O_5	total
201	59.36	0.92	16.52	1.09	5.67	0.12	3.81	6.62	2.50	2.52	0.22	98.99
203	59.65	0.95	16.05	1.00	6.03	0.14	3.72	6.20	2.56	2.43	0.23	98.96
205	61.95	0.86	16.34	1.08	5.07	0.12	2.56	5.43	2.45	2.75	0.19	98.80
207	62.47	0.98	15.78	1.11	5.36	0.12	2.94	5.61	2.14	2.69	0.18	99.29
211	65.36	0.67	15.99	1.29	3.96	0.08	1.19	3.50	2.36	3.50	0.21	98.91
216	65.34	0.78	14.95	0.83	4.41	0.09	1.52	4.55	2.64	3.19	0.22	98.52
218	63.49	0.71	15.78	0.59	4.37	0.11	2.42	4.55	3.55	2.24	0.20	98.01

Rock type: Aplite dikes

sample number	SiO_2	TiO_2	Al_2O_3	Fe_2O_3	FeO	MnO	MgO	CaO	Na_2O	K_2O	P_2O_5	total
133	75.06	0.02	13.83	0.76	1.22	0.03	0.00	0.20	3.94	4.61	0.05	99.72
139	76.27	0.04	12.59	0.10	1.04	0.10	0.00	0.97	3.70	4.27	0.06	99.14
141	75.26	0.06	12.94	0.18	0.95	0.04	0.02	1.01	3.51	4.48	0.04	98.49
150	73.15	0.02	13.68	1.13	1.45	0.01	0.00	0.29	3.89	4.60	0.05	98.27
191	74.42	0.02	13.59	0.96	0.59	0.02	0.00	0.28	3.80	4.53	0.09	98.30

APPENDIX G

Normative mineralogy for each rock type in weight percent

Rock type: Porphyritic quartz monzonite

sample number	qtz	cor	or	ab	an	di	hy	mt	il	ap	total
135	39.15	0.27	20.09	23.35	9.17	0.00	5.72	0.68	0.53	0.23	99.20
137	40.31	0.21	21.75	28.52	6.54	0.00	1.87	0.29	0.13	0.09	99.70
142	30.29	1.04	21.63	27.75	11.19	0.00	6.04	0.65	0.53	0.19	99.31
143	30.02	0.99	21.21	27.42	10.97	0.00	5.44	0.39	0.55	0.21	97.20
144	29.91	0.95	23.70	23.61	10.10	0.00	7.61	0.67	0.78	0.32	97.64
145	34.61	1.58	26.36	26.57	7.65	0.00	3.05	0.42	0.27	0.21	100.71
146	34.44	0.57	20.51	24.54	9.98	0.00	5.84	0.59	0.61	0.21	97.28
148	32.56	1.08	20.15	27.16	10.51	0.00	5.40	0.61	0.47	0.16	98.10
149	36.19	0.73	23.05	28.69	6.89	0.00	2.29	0.16	0.13	0.16	98.28
152	35.83	0.17	23.34	27.50	7.45	0.00	2.69	0.26	0.23	0.14	97.60
161	32.88	1.28	26.36	25.64	9.02	0.00	2.95	0.93	0.38	0.16	99.60
162	35.52	0.43	26.95	31.22	3.98	0.00	1.08	0.51	0.09	0.28	100.05
165	33.60	0.57	24.41	27.75	9.15	0.00	0.57	0.29	0.36	0.19	97.27
166b	32.43	0.00	27.48	31.39	5.47	0.24	0.89	0.22	0.08	0.09	98.29
167	33.20	1.42	24.52	25.30	9.28	0.00	4.13	0.77	0.46	0.21	99.29
173	36.94	0.87	20.98	26.49	11.09	0.00	2.67	0.62	0.30	0.25	100.22
175	32.33	0.53	25.47	24.79	10.56	0.00	4.20	0.83	0.49	0.23	99.43
179	31.71	0.41	29.84	27.08	7.11	0.00	2.62	0.42	0.25	0.12	99.56
186	36.94	1.28	22.99	25.64	8.06	0.00	3.08	0.68	0.38	0.14	99.23
189	34.19	1.45	27.71	23.86	8.04	0.00	3.16	0.55	0.34	0.14	99.45
192	33.19	0.75	26.47	26.65	8.04	0.00	2.91	0.68	0.30	0.14	99.14
194	36.70	0.00	26.30	27.08	7.34	0.15	1.12	0.35	0.15	0.12	99.30
195	29.31	0.60	24.76	26.32	11.59	0.00	4.89	0.71	0.61	0.32	99.11
214	32.68	0.90	23.22	29.11	8.16	0.00	2.92	0.58	0.36	0.19	98.11

Rock type: Porphyritic granodiorite

sample number	qtz	cor	or	ab	an	di	hy	mt	il	ap	total
106	27.30	1.40	20.15	30.38	10.25	0.00	5.92	1.16	0.76	0.32	97.64
108	25.57	0.15	24.52	33.25	10.00	0.00	2.96	0.42	0.63	0.25	97.76
116a	31.73	0.20	23.93	27.42	11.09	0.00	3.24	0.68	0.55	0.19	99.02
127	30.50	1.30	18.50	26.82	13.35	0.00	6.01	0.84	0.93	0.28	98.53
128	30.81	1.28	21.63	25.72	12.51	0.00	4.64	0.99	0.89	0.35	98.82
132	30.76	1.17	21.92	28.69	10.91	0.00	4.36	0.58	0.70	0.30	99.39
134	37.91	1.15	19.91	24.29	9.57	0.00	5.02	0.83	0.49	0.23	99.39
213	30.02	0.61	18.26	29.87	13.75	0.00	4.51	0.94	0.76	0.35	99.07
215	24.41	0.02	17.73	29.95	16.27	0.00	6.89	1.38	1.08	0.44	98.17

Rock type: Fine-grained granodiotite

sample number	qtz	cor	or	ab	an	di	hy	mt	il	ap	total
201	13.65	0.00	14.89	21.15	26.41	2.64	16.40	1.58	1.75	0.51	98.99
203	14.10	0.00	14.36	21.66	25.13	3.41	16.51	1.45	1.80	0.53	98.96
205	19.02	0.00	16.25	20.73	25.47	0.19	13.50	1.57	1.63	0.44	98.80
207	20.58	0.00	15.90	18.11	25.51	0.95	14.53	1.61	1.69	0.42	99.26
211	25.97	0.00	20.68	19.97	15.99	0.00	10.20	1.87	1.27	0.49	98.91
216	23.86	0.00	18.85	22.34	19.52	1.36	9.39	1.20	1.48	0.51	98.52
218	18.65	0.00	13.24	30.04	20.51	0.63	12.28	0.86	1.35	0.46	98.01

Rock type: Aplite dikes

sample number	qtz	cor	or	ab	an	di	hy	mt	il	ap	total
133	33.47	2.11	27.24	33.34	0.67	0.00	1.64	1.10	0.04	0.12	99.72
139	35.61	0.26	25.23	31.31	4.42	0.00	1.95	0.14	0.08	0.14	99.14
141	34.90	0.58	26.47	29.70	4.75	0.00	1.62	0.26	0.11	0.09	98.49
150	31.66	1.89	27.18	32.92	1.11	0.00	1.71	1.64	0.04	0.12	98.27
191	34.50	2.14	26.77	32.15	0.80	0.00	0.29	1.39	0.04	0.21	98.30

APPENDIX H

Rubidium-strontium isotopic data

sample number	Sr (ppm)	Rb (ppm)	$^{87}Sr/^{86}Sr$	$^{87}Rb/^{86}Sr$
128	857	134	0.71284 ± .00034	0.4526
138b	56.6	353	0.73573 ± .00070	18.09
142	365	231	0.71488 ± .00055	1.832
205	608	98.5	0.71370 ± .00016	0.4261
211	702	130	0.71554 ± .00043	0.5361
215	598	185	0.71051 ± .00022	0.8952

452.1475